Article

Neuron

Structural and Functional Remodeling of Amygdala GABAergic Synapses in Associative Fear Learning

Graphical Abstract

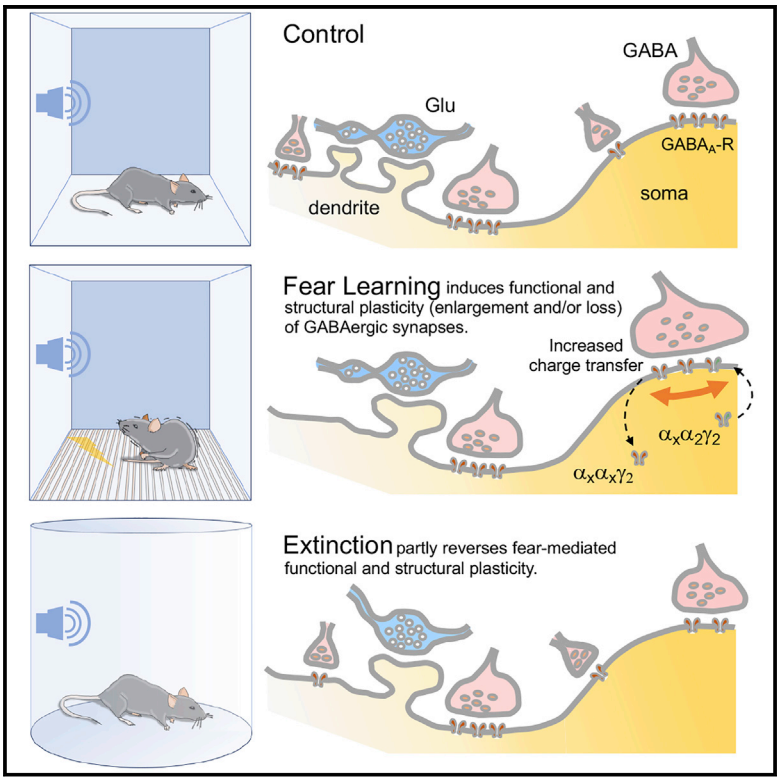

Authors

Yu Kasugai, Elisabeth Vogel, Heide Hörtnagl, ..., Nicolas Singewald, Andreas Lüthi, Francesco Ferraguti

Correspondence

francesco.ferraguti@i-med.ac.at

In Brief

Kasugai et al. show that associative learning, such as fear conditioning, elicits concerted structural and functional plasticity of amygdala GABAergic synapses. This process regulates both somatic and dendritic inhibition and may tune amygdala circuit responses to threats.

Highlights

- Fear learning induces structural and functional plasticity of GABAergic synapses
- Fear learning increases the synaptic fraction of GABA$_A$-Rs containing the α2 subunit
- Plastic changes at GABAergic synapses are long lasting
- Extinction partly reverses fear-mediated structural and functional plasticity

Kasugai et al., 2019, Neuron *104*, 781–794
November 20, 2019
https://doi.org/10.1016/j.neuron.2019.08.013

CellPress

Neuron
Article

Structural and Functional Remodeling of Amygdala GABAergic Synapses in Associative Fear Learning

Yu Kasugai,[1] Elisabeth Vogel,[2] Heide Hörtnagl,[1] Sabine Schönherr,[1] Enrica Paradiso,[1] Markus Hauschild,[3] Georg Göbel,[4] Ivan Milenkovic,[5] Yvan Peterschmitt,[1,5,8] Ramon Tasan,[1] Günther Sperk,[1] Ryuichi Shigemoto,[6] Werner Sieghart,[5] Nicolas Singewald,[3] Andreas Lüthi,[2,7] and Francesco Ferraguti[1,9,*]

[1]Department of Pharmacology, Medical University of Innsbruck, Innsbruck 6020, Austria
[2]Friedrich Miescher Institute for Biomedical Research, Basel 4058, Switzerland
[3]Department of Pharmacology and Toxicology, Institute of Pharmacy and CMBI, University of Innsbruck, Innsbruck 6020, Austria
[4]Department of Medical Statistics, Informatics and Health Economics, Medical University of Innsbruck, Innsbruck 6020, Austria
[5]Center for Brain Research, Department of Molecular Neurosciences, Medical University of Vienna, Vienna 1090, Austria
[6]Institute of Science and Technology Austria, Klosterneuburg 3400, Austria
[7]University of Basel, Basel, Switzerland
[8]Present address: Integrative and Clinical Neurosciences EA 481, Université Bourgogne Franche-Comté, 25000 Besançon, France
[9]Lead Contact
*Correspondence: francesco.ferraguti@i-med.ac.at
https://doi.org/10.1016/j.neuron.2019.08.013

SUMMARY

Associative learning is thought to involve different forms of activity-dependent synaptic plasticity. Although previous studies have mostly focused on learning-related changes occurring at excitatory glutamatergic synapses, we found that associative learning, such as fear conditioning, also entails long-lasting functional and structural plasticity of GABAergic synapses onto pyramidal neurons of the murine basal amygdala. Fear conditioning-mediated structural remodeling of GABAergic synapses was associated with a change in mIPSC kinetics and an increase in the fraction of synaptic benzodiazepine-sensitive (BZD) $GABA_A$ receptors containing the α2 subunit without altering the intrasynaptic distribution and overall amount of BZD-$GABA_A$ receptors. These structural and functional synaptic changes were partly reversed by extinction training. These findings provide evidence that associative learning, such as Pavlovian fear conditioning and extinction, sculpts inhibitory synapses to regulate inhibition of active neuronal networks, a process that may tune amygdala circuit responses to threats.

INTRODUCTION

Long-term changes in synaptic strength and circuit refinement following associative learning have been extensively studied at excitatory glutamatergic synapses (Yuste and Bonhoeffer, 2001; Matsuzaki et al., 2004). Activity-driven structural changes include elimination and formation of synapses, actin-dependent stabilization and enlargement of the postsynaptic density, as well as alterations of the composition of ionotropic glutamate receptors (Holtmaat and Svoboda, 2009; Makino and Malinow, 2009; Caroni et al., 2012; Wang et al., 2014). Plasticity at inhibitory synapses has received much less attention, despite its contribution to the maintenance of the stability, dynamic range, and computational flexibility of neuronal circuits (Castillo et al., 2011; Maffei, 2011; Kullmann et al., 2012).

Pavlovian fear conditioning, also known as classical fear conditioning, is one of the most studied forms of associative learning and depends on synaptic plasticity in the amygdala (Pape and Paré, 2010; Johansen et al., 2011; Bocchio et al., 2017). Not only is it a powerful paradigm to study the neurobiological underpinnings of associative learning in general, but it also represents an important model for understanding the brain mechanisms of normal and pathological fear (Graham and Milad, 2011). It is generally agreed that, during fear conditioning, pyramidal neurons (PNs) in the basolateral amygdala (BLA), comprised of the lateral nucleus (LA) and basal nucleus (BA), undergo complex structural and functional changes at excitatory glutamatergic afferent synapses (Johansen et al., 2011; Tovote et al., 2015), including an increase in spine volume (Ostroff et al., 2010). A large body of evidence suggests that the formation and expression of conditioned fear memories also depend on inhibitory elements within amygdala networks (Ehrlich et al., 2009; Ressler and Maren, 2019). Inhibitory GABAergic circuits are known to gate the acquisition and expression of fear memories not only by tuning excitatory transmission but also by playing more active roles in amygdala intrinsic fear pathways (Wolff et al., 2014; Bazelot et al., 2015). Furthermore, amygdala inhibitory circuits appear to be involved in the formation of new suppressive memories during fear extinction (Herry et al., 2010; Duvarci and Paré, 2014). The critical involvement of the GABAergic system in the regulation of acquired fear is highlighted by the fact that drugs modulating $GABA_A$ receptor ($GABA_A$-R) channels, such as benzodiazepines (BZDs), have been used for decades to treat anxiety disorders. In addition, BZDs have been found to influence

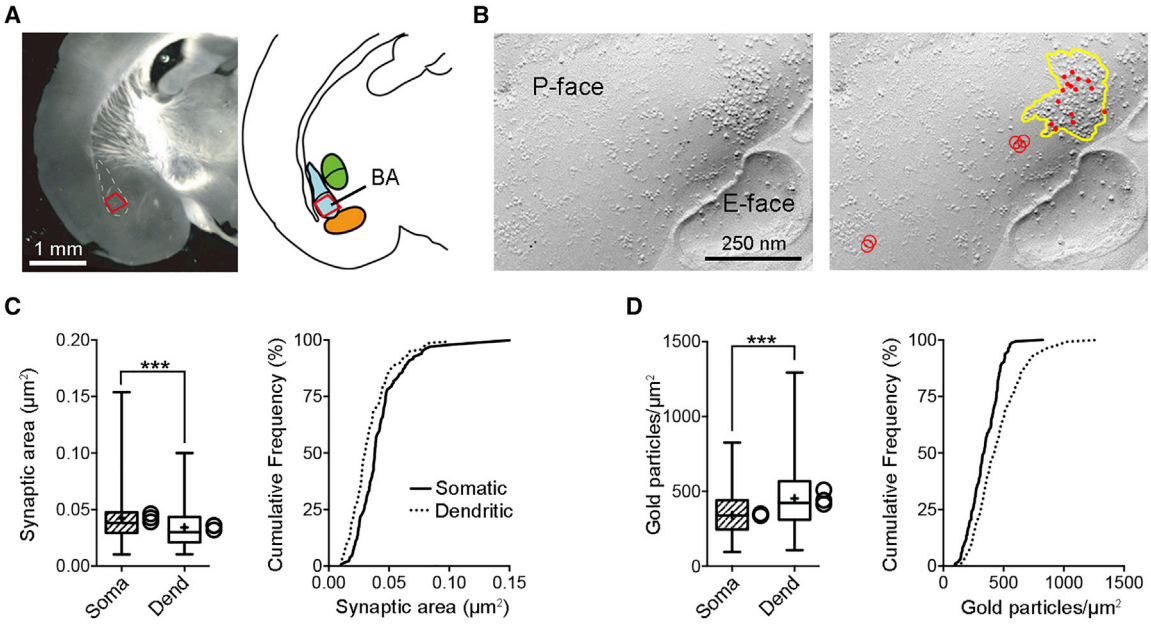

Figure 1. Structural Properties of BZD-Sensitive GABAergic Synapses on BA PNs in Naive Mice

(A) Micrograph of the amygdaloid complex taken from a coronal section of a fixed mouse brain (left panel) and diagram of the amygdala showing the area (red) dissected out for FRIL (right panel). BA, basal nucleus.

(B) Electron micrograph of a GABAergic synapse on the soma of a pyramidal-like neuron in the BA of a naive mouse. The micrograph shows the protoplasmic face (P face) of the soma and the exoplasmic (E) face of an axon terminal. The postsynaptic density of the GABAergic synapse is visible as a cluster of intramembrane particles (area outlined in yellow, right panel) on the replica, which is immunolabeled with 5-nm gold particles identifying the $GABA_A$-γ2 subunit. Gold particles are highlighted by solid red dots when intrasynaptic and red circles when extrasynaptic (right panel). See also Figure S1.

(C) The somatic GABA-PSA was quite variable, ranging from 0.0103 to 0.1540 μm^2, and was significantly larger compared with dendritic synapses (Mann-Whitney test, ***$p < 0.001$). The synaptic area was determined only for full synapses. Synapses were collected from 3 animals, and 44 somatic and 46 dendritic synapses were randomly selected per animal. Because there was no significant difference among animals (Kruskal-Wallis test followed by post hoc Dunn's multiple comparisons test; soma, $p = 0.65$; dendrite, $p = 0.23$), data were pooled. Analysis of the GABA-PSA cumulative frequency distributions by means of two-sample Kolmogorov–Smirnov test showed a highly significant difference (***$p < 0.001$) between somatic and dendritic synapses.

(D) The $GABA_A$-γ2 labeling density is lower in somatic than in dendritic synapses (Mann-Whitney test, ***$p < 0.001$). For density measures, partial synapses were also analyzed (somatic, $n = 165$; dendritic, $n = 234$). Cumulative frequency distributions of the $GABA_A$-γ2 synaptic labeling density show a significant shift to the right of dendritic versus somatic synapses (two-sample Kolmogorov-Smirnov test, ***$p < 0.001$).

Boxplots show the median (line inside the box), mean (+), 25th–75th percentiles (box edges), and minimum and maximum values (whiskers). The mean values of each mouse in a group are shown as empty circles on the right side of the boxplots.

fear responses and extinction learning (Harris and Westbrook, 1995; Hart et al., 2009; Makkar et al., 2010).

So far, studies of GABAergic inhibition during fear conditioning have mostly focused on the control of sensory-evoked activity and the participation and coordination of different interneurons (Capogna, 2014) in inhibition of distinct plasma membrane domains of BLA PNs and in gating of synaptic plasticity at glutamatergic synapses (Wolff et al., 2014; Krabbe et al., 2018). However, whether fear conditioning is associated with structural or functional plasticity of BZD-sensitive GABAergic synapses in the BLA remains largely unknown. Here we addressed this question using a combination of ultrastructural, neurochemical, and electrophysiological approaches in mice.

RESULTS

To investigate whether fear conditioning affects the ultrastructure of GABAergic synapses on PNs of the BA, we used the detergent-solubilized freeze-fracture replica immunolabeling (FRIL) method. This approach allowed us to examine possible changes in synaptic morphology and density of BZD-sensitive $GABA_A$-Rs in relation to associative fear learning. FRIL offers a planar view of the postsynaptic specialization of GABAergic synapses, detectable as a cluster of intramembrane particles (IMPs) at the protoplasmic (P) face of the replica (Figures 1A and 1B; Figures S1A and S1B), which can be labeled for $GABA_A$-R subunits and other integral membrane proteins specific for GABAergic synapses, such as neuroligin 2 (Kasugai et al., 2010). To selectively detect GABAergic synapses containing BZD-sensitive $GABA_A$-Rs, we used highly specific $GABA_A$ γ2 subunit antibodies because the BZD binding pocket is formed at the interface between the γ2 and different α subunits (Olsen and Sieghart, 2008).

First we determined the postsynaptic area of GABAergic synapses (GABA-PSA) and the density of $GABA_A$-γ2 subunits in BA PNs of naive mice because these features have never been described for amygdala neurons. For the estimation of the synaptic area, only completely exposed GABA-PSAs immunolabeled for $GABA_A$-γ2 were sampled, whereas for density measurements, partial synapses were also analyzed. Somatic and

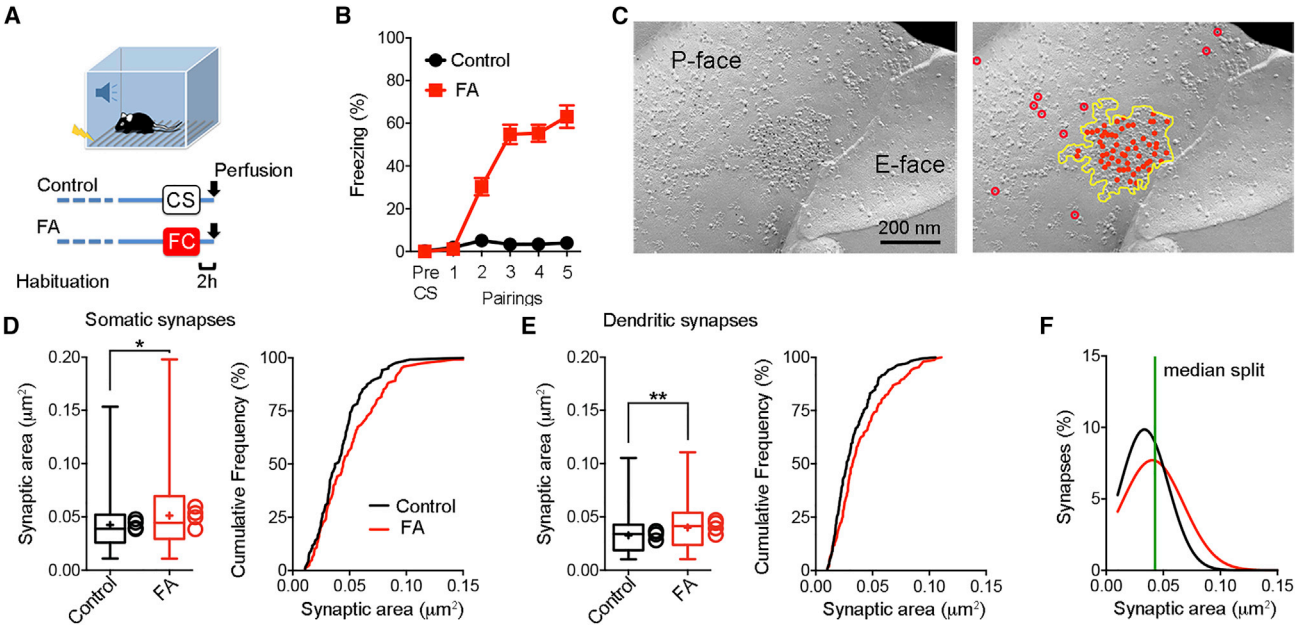

Figure 2. Fear Conditioning Induces Structural Changes of BZD-Sensitive GABAergic Synapses

(A) Schematic diagram of the experimental design. CS, conditioned stimulus; FC, fear conditioning.

(B) Freezing responses of the paired (FA, 5 pairings, 0.7 mA foot shock) and control (exposed to the CS only) groups (n = 9–10 for each group). Data were analyzed by 2-way ANOVA ($F(5,102) = 43.5$, ***$p < 0.001$).

(C) Electron micrograph of a dendritic synapse on a BA PN. In the right panel, the GABA-PSA is outlined in yellow, and the synaptic gold particles are highlighted with red dots and the extrasynaptic ones with red circles.

(D) The somatic GABA-PSA in fear-conditioned mice (n = 120) is larger (Mann-Whitney test, *$p < 0.05$) compared with the control group (n = 120). Synapses were collected from 4 animals/group, and 30 synapses were randomly selected per animal. Because there was no significant difference among animals in each group (Kruskal-Wallis test followed by post hoc Dunn's multiple comparisons test; control, $p = 0.21$; fear, $p = 0.06$), data were pooled. Right panel: GABA-PSA cumulative frequency distributions (two-sample Kolmogorov-Smirnov test, $p = 0.051$).

(E) Fear-conditioned mice also showed larger dendritic GABA-PSAs (n = 112) than controls (n = 112) (Mann-Whitney test; **$p < 0.01$). 28 dendritic synapses were randomly selected per animal; no significant difference was found among animals in each group (Kruskal-Wallis test followed by post hoc Dunn's multiple comparisons test; control, $p = 0.16$; fear, $p = 0.07$), allowing pooling of the data. Right panel: cumulative frequency distributions of the postsynaptic area of dendritic GABAergic synapses (two-sample Kolmogorov-Smirnov test, **$p < 0.01$).

(F) Estimated density function graphs of the somatic GABA-PSAs in the fear-conditioned (FA) and control groups. First, the medians of the somatic synaptic area for the two groups were determined (control, 0.0388; FA, 0.0445) and then averaged to determine the median split (0.0416). Using this cutoff, the delta percentages were obtained, yielding 9.2% below and above the cutoff.

Boxplots show the median (line inside the box), mean (+), 25^{th}–75^{th} percentiles (box edges), and minimum and maximum values (whiskers). The mean values of each mouse in a group are shown as empty circles on the right side of the boxplots.

dendritic synapses were identified by their morphological properties (e.g., exposed area, curvature, and presence of spines; Figures S1A and S1C). To exclude an erratic preservation of $GABA_A$-γ2 in the P face or exoplasmic (E) face of the replica, we assessed the partition properties of these receptors using face-matched replicas and antibodies against epitopes in the N-terminal domain (for the E face) or in the M3-M4 intracellular loop (for the P face) of the $GABA_A$-γ2 subunit (Figures S1B and S1C). A positive correlation between the intrasynaptic density of gold particles in the two faces was observed, indicating a consistent partition of $GABA_A$-γ2-containing receptors in the E and P face (Figure S1D). This allowed us to focus only on the P face, in which the GABA-PSA boundary could be more precisely recognized because of the IMP cluster. To exclude from our quantification the inclusion of extrasynaptic clusters of $GABA_A$-Rs, we took as a threshold for the GABA-PSA the smallest area (0.010 μm^2) measured in the mouse BA from preembedding experiments in which the immunoreactivity for the vesicular GABA transporter (VGAT) was used to unambiguously identify GABAergic synapses (Figure S2).

In naive mice, the dendritic GABA-PSA possessed a smaller area (0.034 ± 0.001 μm^2, Mann-Whitney test, $p < 0.001$) but a higher density of BZD-sensitive $GABA_A$-Rs (452.1 ± 12.9 particles/μm^2, Mann-Whitney test, $p < 0.001$) compared with somatic ones (area, 0.042 ± 0.002 μm^2; density, 340.9 ± 9.6 particles/μm^2; Figures 1C and 1D).

Fear Conditioning Induces Structural and Functional Plasticity at BA GABAergic Synapses

We then tested whether fear conditioning affects the GABA-PSA and density of $GABA_A$-Rs containing the γ2 subunit in BA neurons. Mice were fear conditioned by subjecting them to five pairings of a neutral auditory conditioned stimulus (CS) co-terminating with a foot shock (US), whereas control mice were exposed only to the CS in the conditioning chamber (Figure 2A). Fear-conditioned mice, but not the control group, showed a

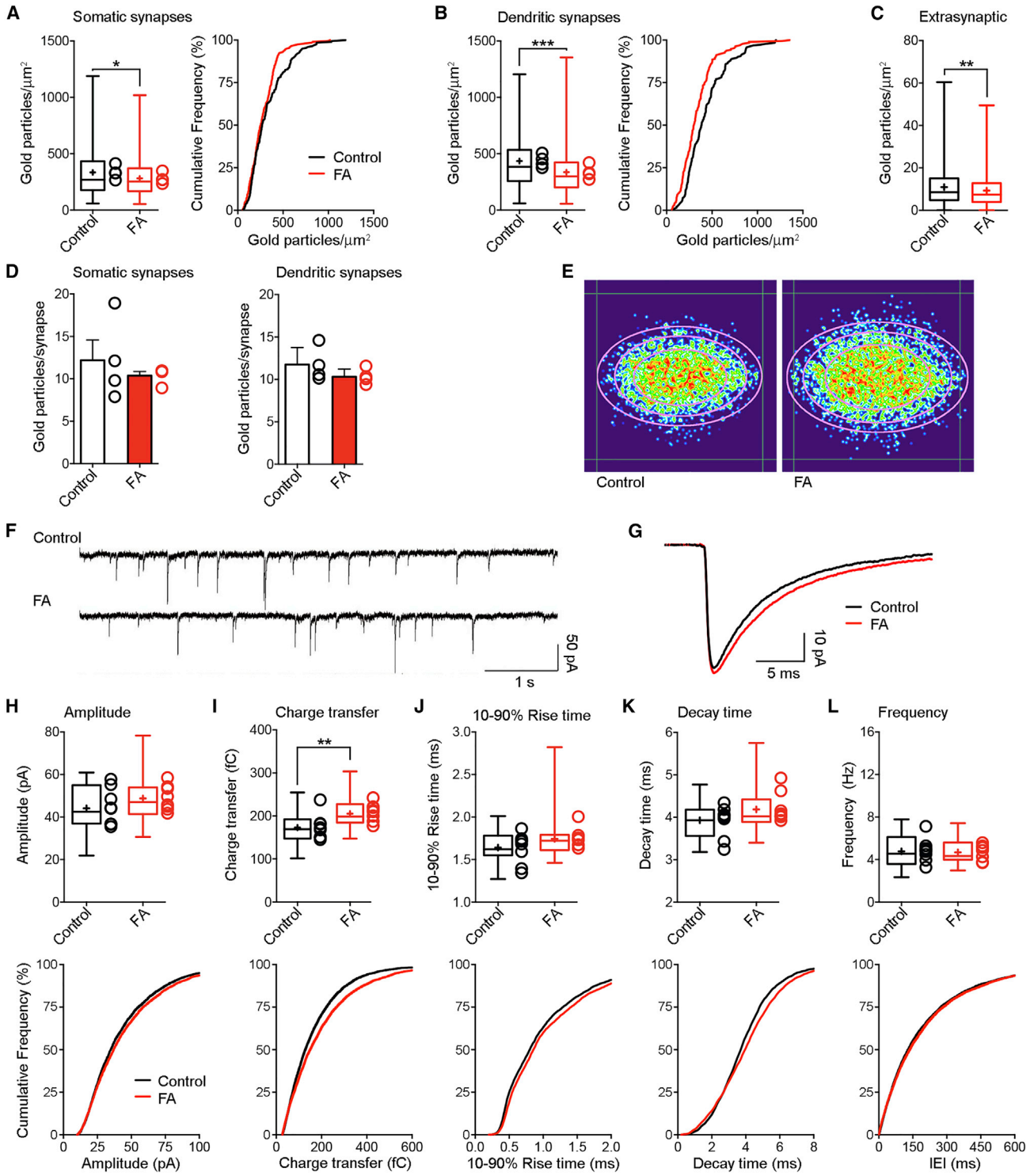

Figure 3. Fear Conditioning Induces Functional Plasticity at BZD-Sensitive GABAergic Synapses

(A) The synaptic $GABA_A$-γ2 labeling density of somatic synapses decreases after fear conditioning (Mann-Whitney test, *$p < 0.05$). Synapses were collected from 4 animals/group, and 50 synapses were randomly selected per animal. Right panel: cumulative frequency distributions of the somatic $GABA_A$-γ2 labeling density (two-sample Kolmogorov-Smirnov test, *$p < 0.05$).

(B) Fear-conditioned mice (n = 192) also showed a reduced dendritic $GABA_A$-γ2 labeling density compared with controls (n = 192, Mann-Whitney test, ***$p < 0.001$). Right panel: cumulative frequency distributions (two-sample Kolmogorov-Smirnov test, ***$p < 0.001$).

(C) The extrasynaptic $GABA_A$-γ2 labeling density decreases after fear conditioning (Mann-Whitney test, **$p < 0.01$).

(legend continued on next page)

progressive increase (2-way ANOVA, $p < 0.001$) in freezing (Figure 2B), demonstrating successful acquisition of a conditioned fear response (FA group). Subsequent to the behavioral testing, mice were returned to their home cages and, 2 h later, processed for FRIL (Figure 2C). Replicas were analyzed by an experimenter blind to the treatment, and data were pooled because they did not differ among animals within each group (Kruskal-Wallis test; somatic synapses control: $p = 0.21$, FA: $p = 0.06$; dendritic synapses control: $p = 0.16$, FA: $p = 0.07$). Fear-conditioned mice showed larger somatic ($0.051 \pm 0.003\ \mu m^2$, Mann-Whitney test, $p < 0.05$) and dendritic ($0.040 \pm 0.002\ \mu m^2$, Mann-Whitney test, $p < 0.01$) GABA-PSAs compared with controls (somatic synapses, $0.042 \pm 0.002\ \mu m^2$; dendritic synapses, $0.032 \pm 0.002\ \mu m^2$; Figures 2D and 2E). Based on the assumption that not all GABAergic synapses in the BA would undergo structural rearrangement after fear conditioning (Han et al., 2007; Reijmers et al., 2007; Grewe et al., 2017), we determined that 9.4% of GABAergic synapses (somatic, ~9.2%; dendritic, ~9.6%) underwent structural rearrangement after fear conditioning by calculating the median split and the delta percentages of the frequency distributions (Figure 2F). The contour of the GABA-PSA was fairly variable (Figure S3A). To determine whether the shift in the GABA-PSA observed after fear conditioning was associated with a change in the shape of the synapses, circularity, roundness, and solidity were examined. None of these shape factors differed between the two groups (Figure S3B), indicating no appreciable changes in GABAergic synaptic morphology. Next we measured the synaptic density of gold particle labeling for $GABA_A$-$\gamma2$. FA mice showed a significant reduction at both somatic (282.6 ± 7.8 particles/μm^2, Mann-Whitney test, $p < 0.05$) and dendritic (336.2 ± 14.2 particles/μm^2, Mann-Whitney test, $p < 0.001$) synapses of the mean $GABA_A$-$\gamma2$ synaptic labeling density compared with controls (somatic, 338.9 ± 7.8 particles/μm^2; dendritic, 435.8 ± 16.9 particles/μm^2; Figures 3A and 3B). Cumulative frequency distributions also revealed a significant shift to the left of the synaptic $GABA_A$-$\gamma2$ labeling density in FA mice (Figure 3B). The extrasynaptic area proximal (up to ~1 μm from the synapse outer border) to GABAergic synapses also showed a significant reduction of the $GABA_A$-$\gamma2$ density in the FA group (Mann-Whitney test, $p < 0.01$; Figure 3C). The density of $GABA_A$-$\gamma2$ in synapses was approximately 30 times higher than in the extrasynaptic area. Despite the different synaptic density, a similar number of gold particles per synapse was observed in the two groups (Mann-Whitney test, somatic $p = 0.40$, dendritic $p = 0.08$; Figure 3D). The number of gold immunoparticles for $GABA_A$-$\gamma2$ in individual synapses was positively correlated with the area of both somatic and dendritic synapses in both groups (Figure S4A), consistent with the results of several previous studies in other cortical areas (Kasugai et al., 2010; Kerti-Szigeti and Nusser, 2016). We further asked whether the intrasynaptic distribution of $GABA_A$-$\gamma2$ could have changed as a result of fear learning. Using a novel approach to analyze the aggregate intrasynaptic dispersion of immunogold labeling (Figure S3C), we showed that fear conditioning did not influence the distribution of $GABA_A$-Rs ($p = 0.11$, chi-square test). We could also observe for the first time that $GABA_A$-$\gamma2$ accrues in the center of the synaptic area, close to the center of gravity (Figure 3E).

To address whether the fear conditioning-induced synaptic and extrasynaptic reduction in $GABA_A$-$\gamma2$ density was due to a decrease in mRNA expression or in the overall number of BZD-binding sites, $GABA_A$-$\gamma2$ transcript levels and the binding of [^{3}H]-flunitrazepam, a positive allosteric modulator at the BZD-binding site, were analyzed by *in situ* hybridization and receptor autoradiography, respectively. No changes in $GABA_A$-$\gamma2$ mRNA levels were detected in the BLA after fear conditioning compared with control animals (Figures S5A and S5B). Also, no changes in the mRNA expression of $GABA_A$-$\alpha1$ and -$\alpha2$ subunits were detected (Figures S5C and S5D). Likewise, [^{3}H]-flunitrazepam binding sites in the BLA were also similar in the two groups (Figure S5E).

To further examine whether synaptic remodeling upon fear conditioning was associated with functional changes, we measured miniature inhibitory postsynaptic currents (mIPSCs) using whole-cell patch-clamp recordings from BA PNs in acute brain slices (Figures 3F–3G). Fear conditioning did not elicit changes in mIPSC frequency (control, 4.76 ± 0.32 Hz; FA, 4.68 ± 0.21 Hz; Mann-Whitney test, $p = 0.90$) or amplitude (control, 44.1 ± 2.02 pA; FA, $48.7 \pm 0.1.91$ pA; Mann-Whitney test, $p = 0.21$; Figures 3H and 3L), whereas the amount of charge

(D) Fear conditioning does not change the number of $GABA_A$-$\gamma2$ gold particles per synapse in either somatic and dendritic synapses (Mann-Whitney test; somatic, $p = 0.40$; dendritic, $p = 0.08$).

(E) Heat plots of the intrasynaptic distribution of $GABA_A$-$\gamma2$ labeling in control and fear-conditioned mice. This model shows that approximately 60% of $\gamma2$-containing $GABA_A$-Rs lie in the inner third of the synaptic area, close to the center of gravity, and that they similarly distribute inside the synapse in control and FA animals. The outer purple ellipsoid describes the average area of BA GABAergic synapses computed for each group (control, n = 344; fear conditioned, n = 396), whereas the other ellipsoids define the inner and middle third of the synaptic area (gold particles in the inner third: control, 60.4%, FA 62.6%; in the middle third: control 28.8%, FA 26.6%; in the outer third: control 8.8%, FA 8.3%; outside of the standard synapse: control 2.4%, FA 2.5%). See also Figure S4.

(F) Example traces illustrating a 6.5-s sweep of mIPSCs recorded from control and fear-conditioned mice.

(G) Examples of averaged mIPSC traces illustrating control and fear acquisition-induced changes in mIPSC kinetics. Traces were obtained by averaging all mIPSCs recorded from one representative cell (control, n = 1,399 mIPSCs; FA, 3 h; n = 594).

(H–L) The amplitude (H), rise time (J), decay time (K), and frequency (L) of mIPSCs in BA PNs are not affected 3 h after fear conditioning. Conversely, the amount of charge conducted per individual mIPSC (I) is enhanced compared with slices obtained from control animals. Data were analyzed by Mann-Whitney test (control, n = 27; FA, n = 31): mIPSC amplitude ($p = 0.21$; control, 44.07 ± 2.02 pA; FA, 48.71 ± 2.09 pA), charge transfer (**$p < 0.01$; control, 173.03 ± 6.77 fC; FA, 205.09 ± 6.74 fC), 10%–90% rise time ($p = 0.12$; control, 1.64 ± 0.04 ms; FA, 1.74 ± 0.04 ms), decay time ($p = 0.09$; control, 3.93 ± 0.09 ms; FA, 4.19 ± 0.09 ms), and frequency ($p = 0.88$; control, 4.76 ± 0.32 Hz; FA, 4.68 ± 0.23 Hz). To construct cumulative plots, 6,669 events per group were randomly selected and pooled. These distribution data were analyzed by two-sample Kolmogorov-Smirnov test: amplitude, ***$p < 0.001$; charge transfer, ***$p < 0.001$; 10%–90% rise time, ***$p < 0.001$; decay time, ***$p < 0.001$; frequency, $p = 0.08$.

Boxplots show the median (line inside the box), mean (+), 25^{th}–75^{th} percentiles (box edges), and minimum and maximum values (whiskers). The mean values of each mouse in a group are shown as empty circles on the right side of the boxplots.

conducted per individual mIPSC (mIPSC charge transfer; FA, 205 ± 7 femtocoulomb [fC]) was significantly enhanced compared with slices obtained from control animals exposed to the CS only (173 ± 7 fC; Mann-Whitney test, $p < 0.01$; Figure 3I). This increase in mIPSC charge transfer could be accounted for by changes in mIPSC kinetics (Figures 3J and 3K).

Taken together, these results show that short-term structural and functional plasticity at BA GABAergic synapses occurs upon acquisition of a conditioned fear response after Pavlovian cued-fear conditioning. Moreover, we show that fear acquisition was also associated with a reduction in surface expression of BZD-sensitive $GABA_A$-Rs that was independent of transcription or translation of $GABA_A$-γ2 and without altering the absolute synaptic content of BZD-sensitive $GABA_A$-Rs.

Fear Conditioning Alters the Synaptic Content of α2-Containing $GABA_A$-R

Because the mIPSCs recorded from BA PNs comprise events originating from both somatic and dendritic inhibitory synapses, we re-examined our mIPSCs by restricting our analysis to events with a fast rise time ($\leq$1 ms), that should derive predominantly from the perisomatic region (Soltesz et al., 1995). A higher mIPSC charge transfer (Mann-Whitney test, $p < 0.05$) was also detected for events with a fast rise time (Figure 4A); however, the magnitude was smaller in comparison with the whole events. This indicates that both somatic and dendritic GABAergic synapses undergo plastic changes upon fear learning.

Because $GABA_A$-Rs composed of different α subunits display diverse gating kinetics (Eyre et al., 2012; Dixon et al., 2014), we hypothesized that the observed change in mIPSC charge transfer might reflect a shift in the subunit composition of synaptic $GABA_A$-Rs following fear conditioning. We, therefore, examined the density of $GABA_A$-α2 subunits in synapses of BA neurons as well as their GABA-PSAs (Figure 4B). Although we could observe plasticity at both somatic and dendritic GABAergic synapses, we decided to focus all of our further investigations on somatic synapses because of the higher diversity of GABAergic interneurons innervating dendritic shafts and potential molecular heterogeneity of these synapses (Klausberger and Somogyi, 2008). Replicas obtained from the same animals analyzed for $GABA_A$-γ2 were used to assess $GABA_A$-α2. The number of gold particles for $GABA_A$-α2 was positively correlated with the GABA-PSA (Figure S4B). An increase in the mean GABA-PSA (Mann-Whitney test, $p < 0.001$) and a shift in the cumulative frequency distribution toward synapses with a larger area were similarly observed in the FA group compared with the control group (Figure 4C). Conversely, no significant difference in the density of the synaptic $GABA_A$-α2 subunit was detected between the 2 groups (Mann-Whitney test, $p = 0.25$; Figure 4D). However, because of the increased GABA-PSA, BA synapses in the FA group should have, as a consequence, a higher overall amount of $GABA_A$-α2 subunits. Indeed, the average number of gold particles per synapse was significantly higher (Mann-Whitney test, $p < 0.01$) in FA animals compared with control mice (Figure 4E). On the other hand, the density of $GABA_A$-α2 within the extrasynaptic area proximal to GABAergic synapses was similar in the 2 experimental groups (Mann-Whitney test, $p = 0.12$; Figure 4F). The delta percentage of the frequency distributions calculated with the median split indicated a structural rearrangement in 14.4% of somatic synapses containing $GABA_A$-α2 subunits (Figure 4G), slightly larger than what we observed for the whole synapses possessing BZD-sensitive $GABA_A$-Rs.

We further performed double labeling experiments for $GABA_A$-α1 and $GABA_A$-α2 to establish whether fear learning alters the rate of synapses containing these subunits (Figure 4H). In control animals, we found that 18% of $GABA_A$-α2-labeled somatic synapses did not contain $GABA_A$-α1, and 2% of $GABA_A$-α1-labeled synapses did not contain $GABA_A$-α2 ($n = 71$). Fear conditioning did not change the rate of synapses containing these subunits (chi-square test, $p = 0.27$; $n = 92$; 12% containing $GABA_A$-α2 only, 4% containing $GABA_A$-α1 only). In double labeling experiments, the steric hindrance produced by antibodies detecting distinct but closely located antigens (e.g., subunits within the same channel) prevents reliable measurement of the relative density of these antigens (Kasugai et al., 2010). Therefore, the respective density of $GABA_A$-α1 and -α2 in double labeling experiments was not analyzed.

Taken together, these findings indicate that fear conditioning alters the gating kinetics of GABAergic perisomatic synapses, most likely by increasing the synaptic content of $GABA_A$-Rs containing the α2 subunit without depleting the extrasynaptic pool and without altering the ratio of synapses possessing $GABA_A$-Rs containing α1 and α2 subunits.

Fear Conditioning-Induced Structural Plasticity Is Long Lasting

To investigate whether the fear conditioning-mediated structural plasticity was only a transitory event, in a separate experiment, mice were fear conditioned or exposed to the CS only and then returned to their home cage for 26 h before being processed for FRIL (Figure 5A). Fear-conditioned mice, but not the control group, showed increased freezing (2-way ANOVA, $p < 0.001$; Figure 5B). Analysis of GABA-PSAs in BA neurons of mice that should have consolidated the fear memory (fear memory [FM] group) showed that structural plasticity could still be observed 26 h after fear conditioning (control, 0.037 ± 0.002 μm^2; FM, 0.045 ± 0.002 μm^2; Mann-Whitney test, $p < 0.05$; Figure 5C). Likewise, the $GABA_A$-γ2 labeling density (FM, 257.4 ± 9.9 particles/μm^2) at somatic synapses remained significantly lower than in control mice (283.4 ± 9.4 particles/μm^2, Mann-Whitney test, $p < 0.05$; Figure 5D). These data reveal that fear conditioning-induced structural plasticity of GABAergic synapses is long lasting.

Fear Conditioning-Induced Structural Plasticity Is Reversed by Extinction Training

In a final set of experiments, we explored whether the synaptic changes induced by fear conditioning were reverted or further reshaped by extinction training. Mice were randomly assigned to 3 groups, 2 of which, on day 1, were fear conditioned, whereas mice in the third group (control) were exposed only to the CS in the conditioning chamber (Figure 6A). Fear-conditioned mice, but not the control group, showed increase freezing (2-way ANOVA, $p < 0.001$; Figure 6B). Following the behavioral test, mice were returned to their home cages. Twenty-four hours later, the two fear-conditioned groups exhibited a marked increase in

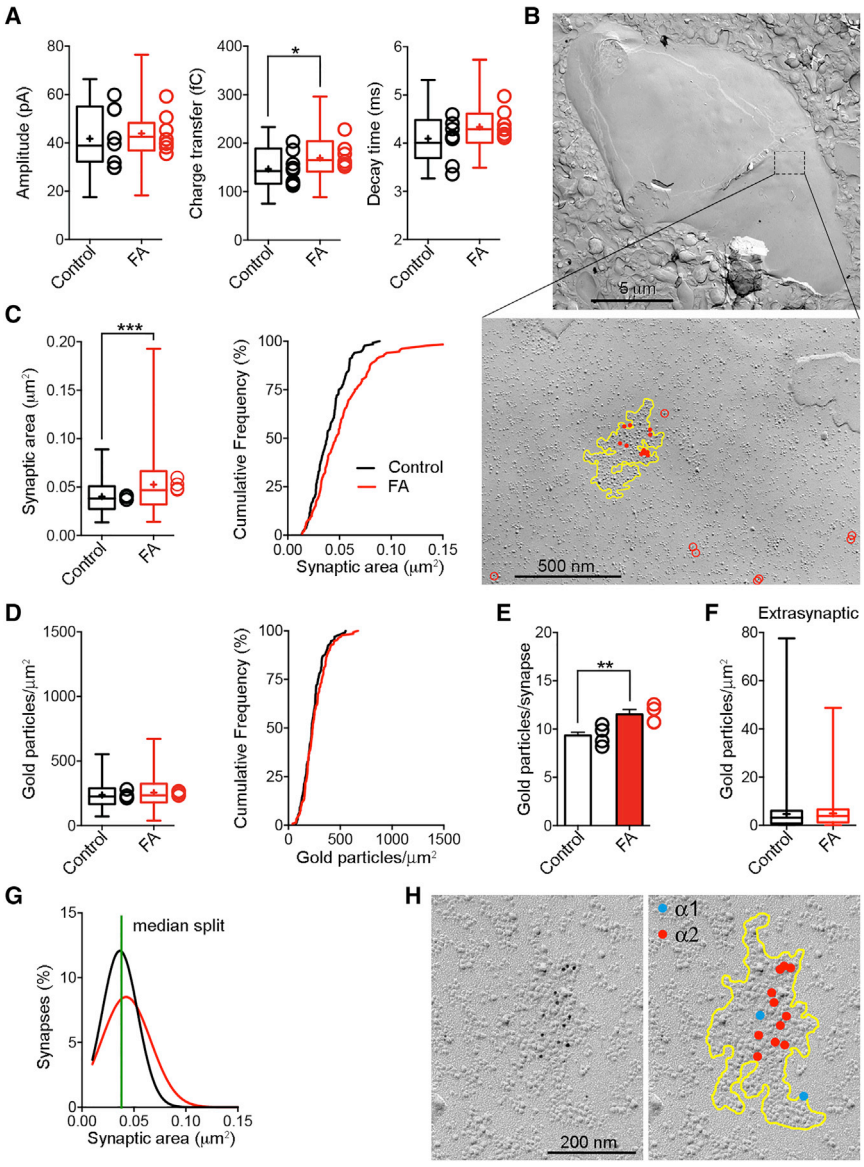

Figure 4. Fear Conditioning Alters the $GABA_A$-R Composition of Perisomatic Synapses

(A) Analysis of mIPSCs with a fast rise time (lower than 1 ms). The amplitude and decay time are not affected by fear conditioning, whereas the charge transfer for these events, most likely originated from the soma, is higher compared with control animals, similar to the total population. Data were analyzed by Mann-Whitney test (control, n = 27; FA, n = 31): mIPSC amplitude (p = 0.59; control 41.81 ± 2.69 pA; FA, 43.86 ± 2.15 pA), charge transfer (*p < 0.05; control, 146.80 ± 7.74 fC; FA, 169.40 ± 7.90 fC), and decay time (p = 0.07; control, 4.10 ± 0.11 ms; FA, 4.34 ± 0.09 ms).

(B) Electron micrograph of a PN soma in the BA of a control mouse. The bottom panel shows high magnification of a GABAergic synapse contained in the area outlined with dashed lines in the top panel. The synapse is immunolabeled with 5-nm gold particles identifying the $GABA_A$-α2 subunit. Gold particles are highlighted by solid red dots when intrasynaptic and red circles when extrasynaptic; the boundary of the synapse is outlined in yellow.

(C) The GABA-PSA of somatic synapses labeled for the α2 subunit is larger in fear-conditioned mice (Mann-Whitney test, ***p < 0.001) than in controls. Synapses were collected from 4 animals/group, and 33 synapses were randomly selected per animal. Because there was no significant difference among animals in each group (Kruskal-Wallis test followed by post hoc Dunn's multiple comparisons test; control, p = 0.84; FA, p = 0.25), data were pooled. Right panel: cumulative frequency distributions of the GABA-PSAs of somatic synapses labeled for the α2 subunit (two-sample Kolmogorov-Smirnov test, **p < 0.01).

(D) The $GABA_A$-α2 labeling density of somatic synapses is similar between control and fear-conditioned mice (Mann-Whitney test; p = 0.39; control, n = 132; FA, n = 132). Right panel: cumulative frequency distributions of the $GABA_A$-α2 synaptic labeling density in somatic synapses (two-sample Kolmogorov-Smirnov test, p = 0.45).

(E) The number of gold particles for $GABA_A$-α2 per somatic synapse is higher in the fear-conditioned mice (n = 132) compared with the control group (n = 132, Mann-Whitney test, **p < 0.01).

(F) The extrasynaptic $GABA_A$-α2 labeling density on the soma did not change after fear conditioning (Mann-Whitney test, p = 0.12).

(G) Estimated density function graphs of the GABA-PSA of somatic synapses labeled for the α2 subunit in FA and control animals. Boxplots show the median (line inside the box), mean (+), 25th–75th percentiles (box edges), and minimum and maximum values (whiskers). The mean values of each mouse in a group are shown as empty circles on the right side of the boxplots.

(H) Electron-micrograph of a GABAergic synapse labeled for the $GABA_A$-α1 (5-nm gold particles) and -α2 subunits (10-nm gold particles) on the soma of a BA PN. Right panel: the postsynaptic density is outlined in yellow, and particles recognizing the $GABA_A$-α1 subunit are highlighted with blue dots and those recognizing the $GABA_A$-α2 subunit with red dots.

freezing behavior when exposed to the CS in a different context. One group was exposed to two CSs (fear memory retrieval; FM+retrieval [Retr] group), whereas the other group underwent extinction of conditioned fear by exposing the mice to 20 non-reinforced CS presentations (extinction [Ext] group), which eventually resulted in low levels (similar to pre-conditioning) of freezing behavior at the end of the extinction training (Figure 6B). Control mice were similarly exposed, on day 2, to 20 presentations of the tone used as a CS (Figure 6A). After the behavioral testing, mice were again returned to their home cages and, 2 h later, processed for FRIL.

An increase of the GABA-PSA of somatic synapses was again observed in FM+Retr mice (0.052 ± 0.002 μm^2) compared with control mice (0.044 ± 0.002 μm^2; Kruskal-Wallis test with Dunn's multiple comparison test, p < 0.001; Figure 6C). Extinction training restored the GABA-PSAs (0.042 ± 0.001 μm^2) to values similar to the control group (Kruskal-Wallis test with Dunn's multiple comparison test, FM+Retr versus Ext mice, p < 0.001;

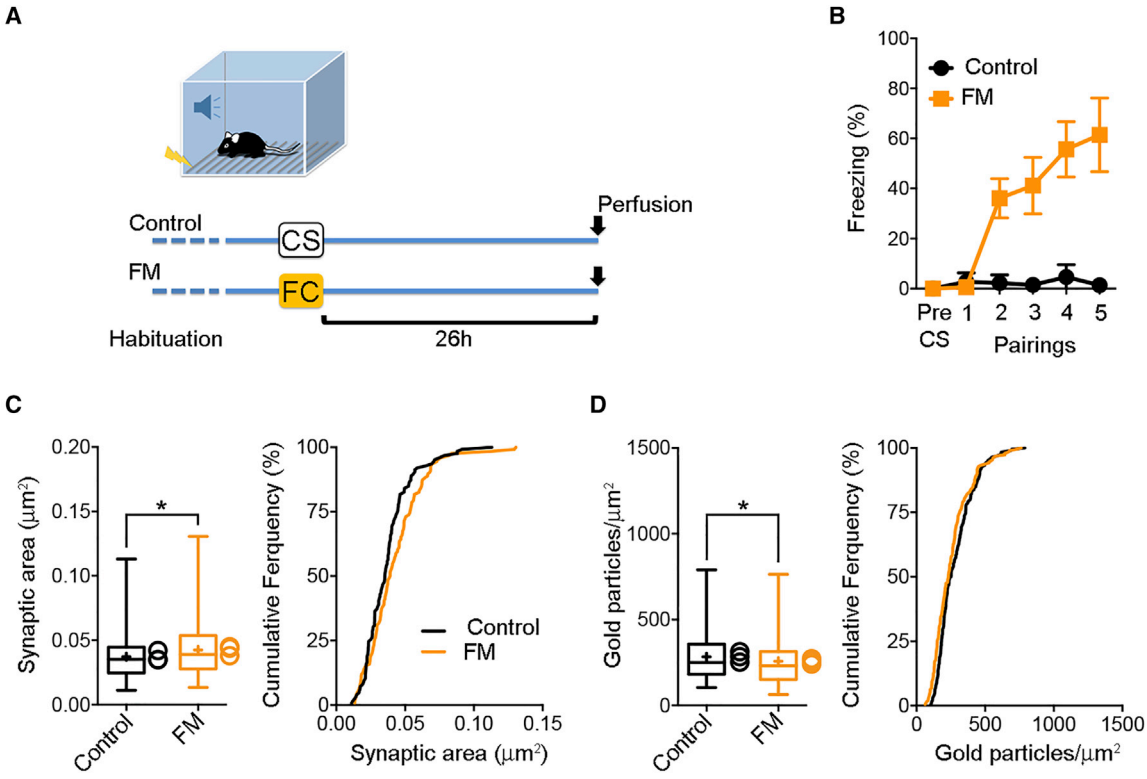

Figure 5. Fear Learning Induces Long-Lasting Structural Plasticity

(A) Schematic diagram of the experimental design.

(B) Freezing responses of the paired (fear memory [FM], 5 pairings, 0.7-mA foot shock) and control (exposed to the CS only) groups (n = 5 for each group). Data were analyzed by 2-way ANOVA ($F(5,48) = 7.559$, $^{***}p < 0.001$).

(C) 26 h after fear conditioning, the GABA-PSA of somatic synapses is still significantly larger compared with control mice (Mann-Whitney test, $^{*}p < 0.05$). Synapses were collected from 3 animals/group, and 42 synapses were randomly selected per animal. Because there was no significant difference among animals in each group (Kruskal-Wallis test followed by post hoc Dunn's multiple comparisons test; control, $p = 0.14$; fear, $p = 0.10$), data were pooled. Right panel: cumulative frequency distributions of the GABA-PSAs of somatic synapses (two-sample Kolmogorov-Smirnov test, $^{*}p < 0.05$).

(D) The $GABA_A$-γ2 labeling density of somatic synapses is also reduced 26 h after fear conditioning (Mann-Whitney test, $^{*}p < 0.05$; control, n = 192; FA, n = 192). Right panel: cumulative frequency distributions of the $GABA_A$-γ2 synaptic labeling density in somatic synapses (two-sample Kolmogorov-Smirnov test, $^{*}p < 0.05$).

Boxplots show the median (line inside the box), mean (+), 25^{th}–75^{th} percentiles (box edges), and minimum and maximum values (whiskers). The mean values of each mouse in the group are shown as empty circles on the right side of the boxplots.

Figure 6C). Consistent with our previous observations, when the density of $GABA_A$-γ2 in somatic synapses was analyzed, a marked reduction was detected in the FM+Retr group (324.9 ± 9.5 particles/μm²) compared with the control group (397.9 ± 11.7 particles/μm²) that did not recover after extinction training (341.1 ± 13.1 particles/μm²; Kruskal-Wallis test with Dunn's multiple comparisons test: FM+Retr versus control, $p < 0.001$; FM+Retr versus Ext, $p = 0.99$; control versus Ext, $p < 0.001$; Figure 6D). Estimation of the number of gold particles per synapse did not reveal differences among the three groups (Kruskal-Wallis test, $p = 0.08$; Figure 6E). Despite a lack of statistical significance, we observed a clear tendency toward a reduction in synaptic BZD-$GABA_A$-Rs following extinction training. In FM+Retr mice, analysis of mIPSCs revealed an increased charge transfer compared with the control group (Kruskal-Wallis with Dunn's multiple comparisons test, $p < 0.05$) but not the Ext group (Figure 6G). The amplitude was similar for all three conditions, whereas a higher mIPSC frequency was observed 24 h after fear conditioning with respect to control mice (Figure 6F; Figures S6B and S6D), suggesting that sustained structural synaptic plasticity may be accompanied by presynaptic functional alterations (Petrini et al., 2014) or by an increase in the overall number of functional GABAergic synapses. Although extinction training did not reverse the increased charge transfer elicited by fear conditioning, it significantly reduced both the decay and 10%–90% rise time (Figures 6H and 6I), indicating that a complex pattern of plastic changes takes place during extinction.

In summary, these findings show bi-directional morphological alterations at BA inhibitory synapses induced by fear conditioning and extinction that are at least in part paralleled by reversible functional changes in synaptic physiology.

DISCUSSION

Studies of learning-dependent structural plasticity have largely focused on excitatory glutamatergic synapses (Caroni et al.,

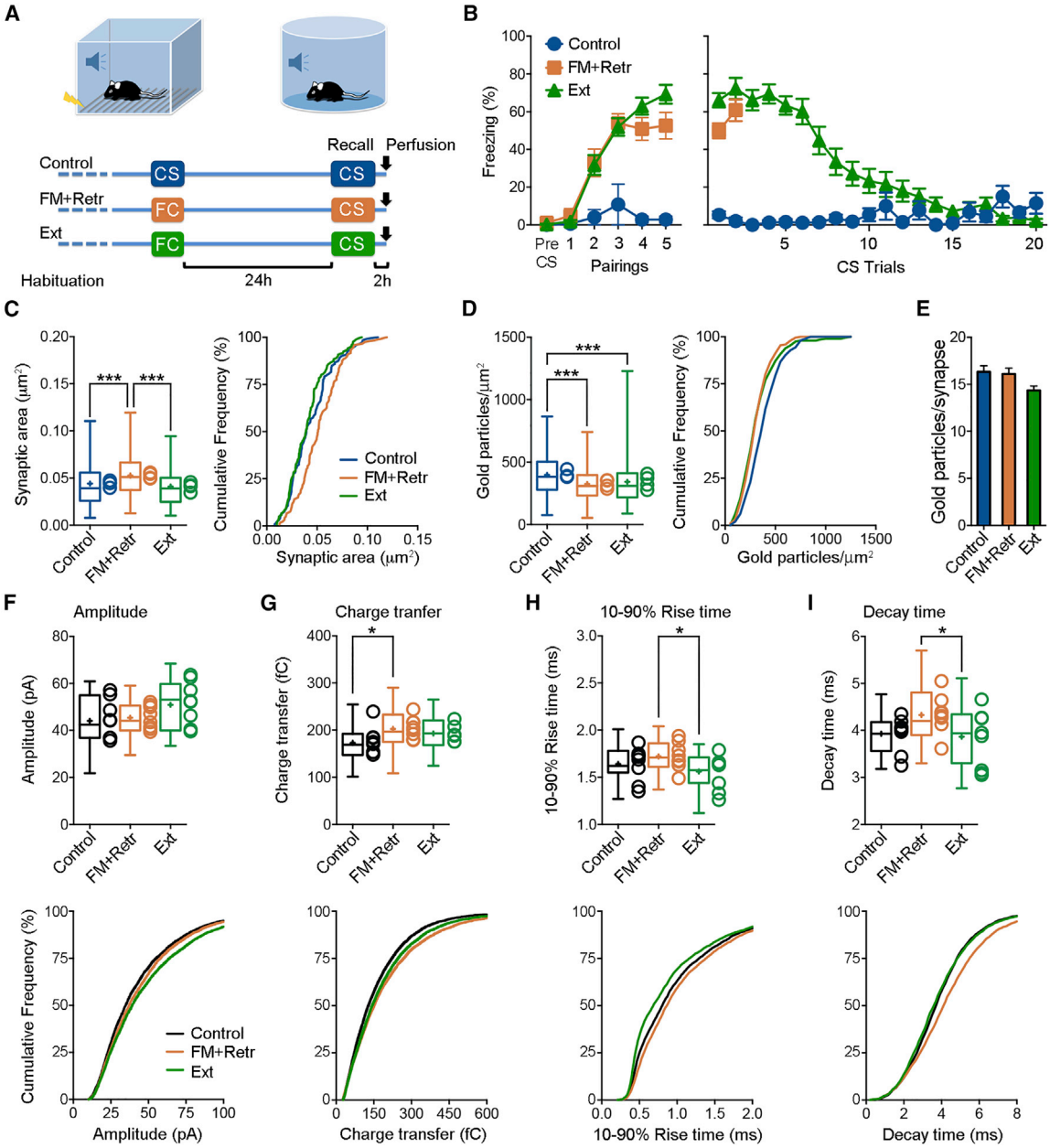

Figure 6. Extinction-Mediated Bi-directional Structural Remodeling of BZD-Sensitive GABAergic Synapses

(A) Schematic diagram of the experimental design for FRIL experiments.

(B) Left panel: freezing responses of the fear memory (n = 8), extinction (n = 9), and control (n = 6) groups. Right panel: freezing responses in mice exposed to fear recall (FM+Retr, 2 CSs), extinction training (Ext, 20 CSs), and 20 CS presentations (control) in a novel environment. Data were analyzed by 2-way ANOVA ($F(10,1628) = 25.37$, $^{***}p < 0.001$).

(C) In FM+Retr mice, the somatic GABA-PSA is again significantly larger compared with control animals (Kruskal-Wallis test followed by post hoc Dunn's multiple comparisons test, $^{***}p < 0.001$) but also with extinguished animals ($^{***}p < 0.001$). Synapses were collected from 4 animals/group, and 33 synapses were randomly selected per animal. Because there was no significant difference among animals in each group (Kruskal-Wallis test; control, $p = 0.05$; FM+Retr, $p = 0.56$; Ext, $p = 0.07$), data were pooled. Right panel: cumulative frequency distributions of the postsynaptic area of GABAergic synapses (two-sample Kolmogorov-Smirnov test; control versus FM+Retr, $^{**}p < 0.01$; Ext versus FM+Retr, $^{***}p < 0.001$; control versus Ext, $p = 0.17$).

(D) Fully consistent with the previous experiments, fear conditioning followed 24 h later by fear retrieval decreases the $GABA_A$-γ2 density in somatic synapses (Kruskal-Wallis test followed by post hoc Dunn's multiple comparisons test; control versus FM+Retr, $^{***}p < 0.001$). The Ext group shows a similar decrease in the $GABA_A$-γ2 density compared with controls (Ext versus control, $^{***}p < 0.001$; Ext versus FM+Retr, $p > 0.99$; n = 196 in each group). Cumulative frequency distributions of the $GABA_A$-γ2 density in somatic synapses (two-sample Kolmogorov-Smirnov test; control versus FM+Retr, $^{***}p < 0.001$; FM+Retr versus Ext, $^{***}p < 0.001$; Ext versus FM+Retr, $p = 0.38$.

(E) The number of gold particles for $GABA_A$-γ2 per synapse was similar among the 3 experimental groups.

(legend continued on next page)

2014; Peters et al., 2017), whereas very little is known about remodeling of GABAergic synapses in mature neural networks. Only recently, *in vivo* imaging of the visual cortex showed synchronized remodeling of spatially clustered dendritic spines and inhibitory synapses over different timescales ranging from hours to days (Chen et al., 2012, 2015; Villa et al., 2016). An emerging view posits that coordinated forms of adaptation of excitation and inhibition are needed to maintain a level of homeostasis necessary to stabilize neuronal and circuit activity (Turrigiano, 2012; Isaacson and Scanziani, 2011; Chiu et al., 2019). Disruption of this balance has been purported to be a pathophysiological mechanism underlying several neuropsychiatric disorders (Lisman, 2012; Nelson and Valakh, 2015).

Fear learning has been associated with changes in spine density and other rearrangements of glutamatergic synapses in the BLA and neocortex (Ostroff et al., 2010; 2012; Lai et al., 2012; Keifer et al., 2015; Yang et al., 2016). Here we show that fear conditioning induces long-lasting concerted structural and functional plasticity of a subset of GABAergic synapses in the BA without modifying the overall synaptic content of BZD-sensitive $GABA_A$-Rs or their subsynaptic distribution. This plastic remodeling of GABAergic synapses occurred at both perisomatic and dendritic synapses and suggests the involvement of different target-specific GABAergic interneurons (Klausberger and Somogyi, 2008; Wolff et al., 2014). In addition, our data are consistent with the notion that the altered mIPSC kinetics mediated by fear conditioning may result from an increase in the synaptic fraction of $GABA_A$-Rs containing the $\alpha 2$ subunit. Finally, our study reveals a remarkable ability of extinction training to offset fear-induced structural and functional changes at GABAergic synapses, unlike other aspects of extinction-associated neuronal plasticity (Maren, 2015).

Fear learning increases the rate of spine elimination in the mouse prefrontal cortex (Lai et al., 2012) and leads to enlargement of excitatory synapses onto spines in the LA (Ostroff et al., 2010; 2012). The higher frequency of GABAergic synapses with a larger area that we observed after fear conditioning can similarly be explained by the removal of subpopulations of small and, presumably, more labile synapses or by inhibition of baseline turnover. Alternatively, the enlarged mean area can also result from synapse stabilization and consequent widening of the synaptic area. Our results are consistent with the observation in rat hippocampal slices that long-term potentiation (LTP), induced by theta-burst stimulation (TBS), causes a coordinated change in the number and size of both excitatory and inhibitory synapses on dendrites of CA1 pyramidal cells (Bourne and Harris, 2011). Similar to our findings, Bourne and Harris (2011) found a decrease in the number and an increase in the size of symmetric synapses 2 h after TBS LTP. Therefore, it can be surmised that the structural remodeling of GABAergic synapses in the BA may depend on both elimination and/or stabilization of synapses. However, to which extent elimination and stabilization contribute to fear conditioning-induced structural plasticity remains to be determined.

Our data indicate that fear learning does not affect the synaptic pool of BZD-sensitive $GABA_A$-Rs, as also supported by no changes in mIPSC amplitude despite a reduction in their density. This can be explained by the preferential accumulation of these $GABA_A$-Rs in the center of the synapse, most likely facing release sites in the active zone, which would result in a similar degree of $GABA_A$-R occupancy per single quantal release of GABA (Perrais and Ropert, 1999; Barberis et al., 2011). To our knowledge, we provide the first demonstration of the subsynaptic localization of $GABA_A$-Rs. Moreover, we reveal, for the first time, that dendritic shaft synapses have a higher density of $GABA_A$-Rs in comparison with perisomatic ones, which denotes a different strength and variability of postsynaptic responses in the operation of BA networks (Hájos et al., 2000). Unlike previous studies (Chhatwal et al., 2005; Heldt and Ressler, 2007), we did not observe significant fear conditioning-mediated alterations in the mRNA expression of $\alpha 1$, $\alpha 2$, or $\gamma 2$ subunits or of [^{3}H]-flunitrazepam binding. This further indicates that, under our experimental conditions, the expression of BZD-sensitive $GABA_A$-Rs remained largely unchanged. However, given the fact that measures of transcription and translation are of "low resolution" and "semi-quantitative" and that the remodeling probably affected a fraction of synapses, our data do not necessarily preclude small alterations in transcription/translation also accounting for the changes observed after fear conditioning.

Here we found that mIPSC amplitude and frequency in BA PNs were not affected within a few hours after fear conditioning, unlike in LA neurons from rats tested with the fear-potentiated startle paradigm (Lin et al., 2009). On the other hand, fear conditioning increased the charge transfer generated by unitary postsynaptic currents, which could be accounted for by changes in mIPSC kinetics. Our findings are consistent with previous evidence showing that the gating kinetics of $GABA_A$-Rs are influenced by different α subunit compositions and that $\alpha 2$-containing $GABA_A$-Rs exhibit a slower decay time of IPSCs than those mediated by $\alpha 1$-containing $GABA_A$-Rs (Eyre et al., 2012; Dixon et al., 2014). Similar to rat CA1 pyramidal cells (Kasugai et al., 2010; Kerti-Szigeti and Nusser, 2016),

(F–I) FM+Retr mice have a higher charge transfer (G) compared with controls, whereas the amplitude (F), rise time (H), and decay time (I) of mIPSCs in BA PNs do not statistically differ between the two groups. Conversely, in Ext mice, both the rise (H) and decay time (I) were significantly lower than for the FM+Retr group. Data were analyzed by Kruskal-Wallis test followed by post hoc Dunn's multiple comparisons test (control, n = 27; FA, n = 31; Ext, n = 26): amplitude, control versus FM+Retr $p > 0.99$, control versus Ext $p = 0.13$, Ext versus FM+Retr $p = 0.27$ (control 44.07 ± 2.02 pA, FM+Retr 45.34 ± 1.439 pA, Ext 50.92 ± 2.25 pA); charge transfer, control versus FM+Retr $^*p < 0.05$, control versus Ext $p = 0.14$, Ext versus FM+Retr $p > 0.99$ (control 173.03 ± 6.77 fC; FM+Retr 202.61 ± 6.74 fC; Ext 192.88 ± 6.65 fC); 10%–90% rise time, control versus FM+Retr $p = 0.35$, control versus Ext $p = 0.67$, Ext versus FM+Retr $^*p < 0.05$ (control 1.64 ± 0.04 ms; FM+Retr 1.72 ± 0.03 ms; Ext 1.56 ± 0.04 ms); decay time, control versus FM+Retr $p = 0.08$, control versus Ext $p > 0.99$, Ext versus FM+Retr $^*p < 0.05$ (control 3.93 ± 0.09 ms; FM+Retr 4.33 ± 0.12 ms; Ext 3.86 ± 0.13 ms). Data are given as mean ± SEM. To construct cumulative plots, 6,669 events per group were randomly selected and pooled.

Boxplots show the median (line inside the box), mean (+), 25th–75th percentiles (box edges), and minimum and maximum values (whiskers). The mean values of each mouse in a group are shown as empty circles on the right side of the boxplots.

we show that more than 80% of GABAergic synapses on BA PNs contain $GABA_A$-Rs possessing α1 and α2 subunits. Although fear conditioning did not change the ratio of synapses possessing $GABA_A$-Rs containing these α subunits, our data show that fear learning results in an increased number of $GABA_A$-α2 per synapse, fully consistent with the observed increase in charge transfer and a prevailing effect of α2 subunits on $GABA_A$ channel properties (del Río et al., 2001; Eyre et al., 2012). Currently, we do not know whether fear conditioning also mediates changes in $GABA_A$-α3, which is highly expressed in the mouse BA (Hörtnagl et al., 2013). Despite many attempts, we have been unable to identify an antibody against this subunit working on replicas. A shift in synaptic $GABA_A$ subunit composition following fear conditioning may represent a homeostatic adjustment of the responsiveness and function of BA neuronal networks upon exposure to aversive environmental conditions (Fritschy and Panzanelli, 2014). Previous studies have shown that both α1- and α2-containing $GABA_A$-Rs are necessary for BZDs to reduce conditioned fear, whereas, in unconditioned tests of anxiety, only α2-containing receptors are required for BZD-induced anxiolysis (Smith et al., 2012). $GABA_A$-Rs containing the α2 subunit may thus be key molecular determinants in regulating the response to threats.

An intriguing outcome of our study is the bidirectional structural remodeling of BA GABAegic synapses after fear conditioning and extinction. This is consistent with recent findings of extinction-induced remodeling of BLA parvalbumin-expressing interneurons, which gives rise to apparently increased perisomatic inhibition of fear-activated PNs (Trouche et al., 2013) and a shift in the balance between competitive fear and extinction memory circuits (Davis et al., 2017). On the other hand, we observed that extinction training did not reverse the fear learning-mediated reduction in intrasynaptic density of BZD-sensitive $GABA_A$-Rs and was congruently unable to offset the enhanced charge transfer, although it influenced the rise and decay time. Our data, therefore, suggest that extinction elicits distinct forms of synaptic plasticity besides counterbalancing the structural synaptic remodeling observed upon fear conditioning. The current prevalent view is that extinction is an active new learning process that competes with the original CS-US association in determining behavior (Bouton, 2004). However, there is also evidence showing that extinction can involve unlearning or erasure components (Maren, 2015). For instance, extinction reversed fear conditioning-induced dendritic spine remodeling (Lai et al., 2012; 2018) as well as potentiation of synaptic efficacy and enhanced surface expression of AMPA receptors at excitatory synapses (Kim et al., 2007). Our study shows that this may also be the case for GABAergic synapses and corroborates the view that, during extinction, both new learning and unlearning mechanisms may occur in parallel.

In conclusion, we provide evidence of novel mechanisms by which associative learning, such as Pavlovian fear conditioning and extinction, sculpts inhibitory synapses to tune the responsiveness and function of active neuronal networks and, possibly, to regulate plasticity and learning rules upon further exposure to threats. The exact functional implications of these modifications for fear and extinction learning remain to be determined. However, an integrated model of fear and anxiety may be exemplified as a delicate balance between overactive excitatory inputs signaling a threat and intrinsic inhibitory control mechanisms related to the appropriate representation of the emotional salience of the stimuli. Within this framework, enlargement of the postsynaptic area or selective conservation of GABAergic synapses with a larger area could act as a metaplasticity mechanism to allow incorporation of more $GABA_A$-Rs to offset particularly intense or prolonged adverse stimuli, as in the case of sustained fear. Indeed, increased synaptic length has been reported for LA GABAergic synapses in GAD65-deficient mice (Lange et al., 2014), which show generalization of learned fear responses (Bergado-Acosta et al., 2008) and impaired fear extinction (Sangha et al., 2012).

Therefore, we suggest that the fear-mediated long-term structural and functional remodeling of BZD-sensitive GABAergic synapses in the BA, including a shift in the synaptic $GABA_A$-Rs containing the α2 subunit, known to predominantly mediate the anxiolytic effect of BZD (Löw et al., 2000), instructs excitatory/inhibitory homeostatic balance and enables reorganization of inhibitory circuit participation through both Hebbian and non-Hebbian forms of plasticity.

STAR★METHODS

Detailed methods are provided in the online version of this paper and include the following:

- KEY RESOURCES TABLE
- LEAD CONTACT AND MATERIALS AVAILABILITY
- EXPERIMENTAL MODEL AND SUBJECT DETAILS
- METHOD DETAILS
  - Fear conditioning
  - Pre-embedding electron microscopy
  - Freeze-fracture replica immunolabeling
  - Image analysis of electron microscopy images
  - Brain slice electrophysiology
  - *In situ* hybridization
  - Autoradiography
- QUANTIFICATION AND STATISTICAL ANALYSIS
- DATA AND CODE AVAILABILITY

SUPPLEMENTAL INFORMATION

Supplemental Information can be found online at https://doi.org/10.1016/j.neuron.2019.08.013.

ACKNOWLEDGMENTS

The authors thank Gabi Schmid for excellent technical support. We also thank Dr. H. Harada, Dr. W. Kaufmann, and Dr. B. Kapelari for testing the specificity of some of the antibodies used in this study on replicas. Funding was provided by the Austrian Science Fund (Fonds zur Förderung der Wissenschaftlichen Forschung) Sonderforschungsbereich grants F44-17 (to F.|F.), F44-10 and P25375-B24 (to N.S.), and P26680 (to G.S.) and by the Novartis Research Foundation and the Swiss National Science Foundation (to A.L). We also thank Prof. M. Capogna for reading a previous version of the manuscript.

AUTHOR CONTRIBUTIONS

Conceptualization, F.F. and A.L.; Methodology, Y.K. and F.F.; Validation, Y.K. and E.V.; Formal Analysis, Y.K., E.V., H.H., E.P., M.H., G.G., R.T., A.L., and F.F.; Investigation, Y.K., E.V., H.H., S.S., E.P., M.H., I.M., Y.P., and F.F.; Resources, G.S., R.S., W.S., N.S., A.L., and F.F.; Writing – Original Draft, Y.K., A.L., and F.F.; Writing – Review & Editing, Y.K., H.H., G.S., R.S., W.S., N.S., A.L., and F.F.; Visualization, Y.K., A.L., and F.F.; Project Administration, A.L. and F.F.; Funding Acquisition, G.S., A.L., and F.F.

DECLARATION OF INTERESTS

The authors declare no competing interests.

Received: May 29, 2019
Revised: July 9, 2019
Accepted: August 7, 2019
Published: September 19, 2019

REFERENCES

Barberis, A., Petrini, E.M., and Mozrzymas, J.W. (2011). Impact of synaptic neurotransmitter concentration time course on the kinetics and pharmacological modulation of inhibitory synaptic currents. Front. Cell. Neurosci. *5*, 6.

Bazelot, M., Bocchio, M., Kasugai, Y., Fischer, D., Dodson, P.D., Ferraguti, F., and Capogna, M. (2015). Hippocampal Theta Input to the Amygdala Shapes Feedforward Inhibition to Gate Heterosynaptic Plasticity. Neuron *87*, 1290–1303.

Bergado-Acosta, J.R., Sangha, S., Narayanan, R.T., Obata, K., Pape, H.C., and Stork, O. (2008). Critical role of the 65-kDa isoform of glutamic acid decarboxylase in consolidation and generalization of Pavlovian fear memory. Learn. Mem. *15*, 163–171.

Bissière, S., Humeau, Y., and Lüthi, A. (2003). Dopamine gates LTP induction in lateral amygdala by suppressing feedforward inhibition. Nat. Neurosci. *6*, 587–592.

Bocchio, M., Nabavi, S., and Capogna, M. (2017). Synaptic Plasticity, Engrams, and Network Oscillations in Amygdala Circuits for Storage and Retrieval of Emotional Memories. Neuron *94*, 731–743.

Bourne, J.N., and Harris, K.M. (2011). Coordination of size and number of excitatory and inhibitory synapses results in a balanced structural plasticity along mature hippocampal CA1 dendrites during LTP. Hippocampus *21*, 354–373.

Bouton, M.E. (2004). Context and behavioral processes in extinction. Learn. Mem. *11*, 485–494.

Capogna, M. (2014). GABAergic cell type diversity in the basolateral amygdala. Curr. Opin. Neurobiol. *26*, 110–116.

Caroni, P., Donato, F., and Muller, D. (2012). Structural plasticity upon learning: regulation and functions. Nat. Rev. Neurosci. *13*, 478–490.

Caroni, P., Chowdhury, A., and Lahr, M. (2014). Synapse rearrangements upon learning: from divergent-sparse connectivity to dedicated sub-circuits. Trends Neurosci. *37*, 604–614.

Castillo, P.E., Chiu, C.Q., and Carroll, R.C. (2011). Long-term plasticity at inhibitory synapses. Curr. Opin. Neurobiol. *21*, 328–338.

Chen, J.L., Villa, K.L., Cha, J.W., So, P.T., Kubota, Y., and Nedivi, E. (2012). Clustered dynamics of inhibitory synapses and dendritic spines in the adult neocortex. Neuron *74*, 361–373.

Chen, S.X., Kim, A.N., Peters, A.J., and Komiyama, T. (2015). Subtype-specific plasticity of inhibitory circuits in motor cortex during motor learning. Nat. Neurosci. *18*, 1109–1115.

Chhatwal, J.P., Myers, K.M., Ressler, K.J., and Davis, M. (2005). Regulation of gephyrin and $GABA_A$ receptor binding within the amygdala after fear acquisition and extinction. J. Neurosci. *25*, 502–506.

Chiu, C.Q., Barberis, A., and Higley, M.J. (2019). Preserving the balance: diverse forms of long-term GABAergic synaptic plasticity. Nat. Rev. Neurosci. *20*, 272–281.

Davis, P., Zaki, Y., Maguire, J., and Reijmers, L.G. (2017). Cellular and oscillatory substrates of fear extinction learning. Nat. Neurosci. *20*, 1624–1633.

del Río, J.C., Araujo, F., Ramos, B., Ruano, D., and Vitorica, J. (2001). Prevalence between different alpha subunits performing the benzodiazepine binding sites in native heterologous GABA(A) receptors containing the alpha2 subunit. J. Neurochem. *79*, 183–191.

Dixon, C., Sah, P., Lynch, J.W., and Keramidas, A. (2014). GABAA receptor α and γ subunits shape synaptic currents via different mechanisms. J. Biol. Chem. *289*, 5399–5411.

Dobi, A., Sartori, S.B., Busti, D., Van der Putten, H., Singewald, N., Shigemoto, R., and Ferraguti, F. (2013). Neural substrates for the distinct effects of presynaptic group III metabotropic glutamate receptors on extinction of contextual fear conditioning in mice. Neuropharmacology *66*, 274–289.

Duvarci, S., and Paré, D. (2014). Amygdala microcircuits controlling learned fear. Neuron *82*, 966–980.

Ehrlich, I., Humeau, Y., Grenier, F., Ciocchi, S., Herry, C., and Lüthi, A. (2009). Amygdala inhibitory circuits and the control of fear memory. Neuron *62*, 757–771.

Eyre, M.D., Renzi, M., Farrant, M., and Nusser, Z. (2012). Setting the time course of inhibitory synaptic currents by mixing multiple GABA(A) receptor α subunit isoforms. J. Neurosci. *32*, 5853–5867.

Fritschy, J.M., and Panzanelli, P. (2014). $GABA_A$ receptors and plasticity of inhibitory neurotransmission in the central nervous system. Eur. J. Neurosci. *39*, 1845–1865.

Graham, B.M., and Milad, M.R. (2011). The study of fear extinction: implications for anxiety disorders. Am. J. Psychiatry *168*, 1255–1265.

Grewe, B.F., Gründemann, J., Kitch, L.J., Lecoq, J.A., Parker, J.G., Marshall, J.D., Larkin, M.C., Jercog, P.E., Grenier, F., Li, J.Z., et al. (2017). Neural ensemble dynamics underlying a long-term associative memory. Nature *543*, 670–675.

Hájos, N., Katona, I., Naiem, S.S., MacKie, K., Ledent, C., Mody, I., and Freund, T.F. (2000). Cannabinoids inhibit hippocampal GABAergic transmission and network oscillations. Eur. J. Neurosci. *12*, 3239–3249.

Han, J.H., Kushner, S.A., Yiu, A.P., Cole, C.J., Matynia, A., Brown, R.A., Neve, R.L., Guzowski, J.F., Silva, A.J., and Josselyn, S.A. (2007). Neuronal competition and selection during memory formation. Science *316*, 457–460.

Harris, J.A., and Westbrook, R.F. (1995). Effects of benzodiazepine microinjection into the amygdala or periaqueductal gray on the expression of conditioned fear and hypoalgesia in rats. Behav. Neurosci. *109*, 295–304.

Hart, G., Harris, J.A., and Westbrook, R.F. (2009). Systemic or intra-amygdala injection of a benzodiazepine (midazolam) impairs extinction but spares re-extinction of conditioned fear responses. Learn. Mem. *16*, 53–61.

Heldt, S.A., and Ressler, K.J. (2007). Training-induced changes in the expression of GABAA-associated genes in the amygdala after the acquisition and extinction of Pavlovian fear. Eur. J. Neurosci. *26*, 3631–3644.

Herry, C., Ciocchi, S., Senn, V., Demmou, L., Müller, C., and Lüthi, A. (2008). Switching on and off fear by distinct neuronal circuits. Nature *454*, 600–606.

Herry, C., Ferraguti, F., Singewald, N., Letzkus, J.J., Ehrlich, I., and Lüthi, A. (2010). Neuronal circuits of fear extinction. Eur. J. Neurosci. *31*, 599–612.

Holtmaat, A., and Svoboda, K. (2009). Experience-dependent structural synaptic plasticity in the mammalian brain. Nat. Rev. Neurosci. *10*, 647–658.

Hörtnagl, H., Tasan, R.O., Wieselthaler, A., Kirchmair, E., Sieghart, W., and Sperk, G. (2013). Patterns of mRNA and protein expression for 12 GABAA receptor subunits in the mouse brain. Neuroscience *236*, 345–372.

Isaacson, J.S., and Scanziani, M. (2011). How inhibition shapes cortical activity. Neuron *72*, 231–243.

Johansen, J.P., Cain, C.K., Ostroff, L.E., and LeDoux, J.E. (2011). Molecular mechanisms of fear learning and memory. Cell *147*, 509–524.

Kasugai, Y., Swinny, J.D., Roberts, J.D., Dalezios, Y., Fukazawa, Y., Sieghart, W., Shigemoto, R., and Somogyi, P. (2010). Quantitative localisation of synaptic and extrasynaptic $GABA_A$ receptor subunits on hippocampal pyramidal cells by freeze-fracture replica immunolabelling. Eur. J. Neurosci. *32*, 1868–1888.

Keifer, O.P., Jr., Hurt, R.C., Gutman, D.A., Keilholz, S.D., Gourley, S.L., and Ressler, K.J. (2015). Voxel-based morphometry predicts shifts in dendritic spine density and morphology with auditory fear conditioning. Nat. Commun. *6*, 7582.

Kerti-Szigeti, K., and Nusser, Z. (2016). Similar GABAA receptor subunit composition in somatic and axon initial segment synapses of hippocampal pyramidal cells. eLife *5*, e18426.

Kim, J., Lee, S., Park, K., Hong, I., Song, B., Son, G., Park, H., Kim, W.R., Park, E., Choe, H.K., et al. (2007). Amygdala depotentiation and fear extinction. Proc. Natl. Acad. Sci. USA *104*, 20955–20960.

Klausberger, T., and Somogyi, P. (2008). Neuronal diversity and temporal dynamics: the unity of hippocampal circuit operations. Science *321*, 53–57.

Krabbe, S., Gründemann, J., and Lüthi, A. (2018). Amygdala Inhibitory Circuits Regulate Associative Fear Conditioning. Biol. Psychiatry *83*, 800–809.

Kullmann, D.M., Moreau, A.W., Bakiri, Y., and Nicholson, E. (2012). Plasticity of inhibition. Neuron *75*, 951–962.

Lai, C.S., Franke, T.F., and Gan, W.B. (2012). Opposite effects of fear conditioning and extinction on dendritic spine remodelling. Nature *483*, 87–91.

Lai, C.S.W., Adler, A., and Gan, W.B. (2018). Fear extinction reverses dendritic spine formation induced by fear conditioning in the mouse auditory cortex. Proc. Natl. Acad. Sci. USA *115*, 9306–9311.

Lange, M.D., Jüngling, K., Paulukat, L., Vieler, M., Gaburro, S., Sosulina, L., Blaesse, P., Sreepathi, H.K., Ferraguti, F., and Pape, H.C. (2014). Glutamic acid decarboxylase 65: a link between GABAergic synaptic plasticity in the lateral amygdala and conditioned fear generalization. Neuropsychopharmacology *39*, 2211–2220.

Lin, H.C., Mao, S.C., and Gean, P.W. (2009). Block of gamma-aminobutyric acid-A receptor insertion in the amygdala impairs extinction of conditioned fear. Biol. Psychiatry *66*, 665–673.

Lisman, J. (2012). Excitation, inhibition, local oscillations, or large-scale loops: what causes the symptoms of schizophrenia? Curr. Opin. Neurobiol. *22*, 537–544.

Löw, K., Crestani, F., Keist, R., Benke, D., Brünig, I., Benson, J.A., Fritschy, J.M., Rülicke, T., Bluethmann, H., Möhler, H., and Rudolph, U. (2000). Molecular and neuronal substrate for the selective attenuation of anxiety. Science *290*, 131–134.

Maffei, A. (2011). The many forms and functions of long term plasticity at GABAergic synapses. Neural Plast. *2011*, 254724.

Makino, H., and Malinow, R. (2009). AMPA receptor incorporation into synapses during LTP: the role of lateral movement and exocytosis. Neuron *64*, 381–390.

Makkar, S.R., Zhang, S.Q., and Cranney, J. (2010). Behavioral and neural analysis of GABA in the acquisition, consolidation, reconsolidation, and extinction of fear memory. Neuropsychopharmacology *35*, 1625–1652.

Maren, S. (2015). Out with the old and in with the new: Synaptic mechanisms of extinction in the amygdala. Brain Res. *1621*, 231–238.

Matsuzaki, M., Honkura, N., Ellis-Davies, G.C., and Kasai, H. (2004). Structural basis of long-term potentiation in single dendritic spines. Nature *429*, 761–766.

Nelson, S.B., and Valakh, V. (2015). Excitatory/Inhibitory Balance and Circuit Homeostasis in Autism Spectrum Disorders. Neuron *87*, 684–698.

Olsen, R.W., and Sieghart, W. (2008). International Union of Pharmacology. LXX. Subtypes of gamma-aminobutyric acid(A) receptors: classification on the basis of subunit composition, pharmacology, and function. Update. Pharmacol. Rev. *60*, 243–260.

Ostroff, L.E., Cain, C.K., Bedont, J., Monfils, M.H., and Ledoux, J.E. (2010). Fear and safety learning differentially affect synapse size and dendritic translation in the lateral amygdala. Proc. Natl. Acad. Sci. USA *107*, 9418–9423.

Ostroff, L.E., Cain, C.K., Jindal, N., Dar, N., and Ledoux, J.E. (2012). Stability of presynaptic vesicle pools and changes in synapse morphology in the amygdala following fear learning in adult rats. J. Comp. Neurol. *520*, 295–314.

Pape, H.C., and Paré, D. (2010). Plastic synaptic networks of the amygdala for the acquisition, expression, and extinction of conditioned fear. Physiol. Rev. *90*, 419–463.

Perrais, D., and Ropert, N. (1999). Effect of zolpidem on miniature IPSCs and occupancy of postsynaptic GABAA receptors in central synapses. J. Neurosci. *19*, 578–588.

Peters, A.J., Liu, H., and Komiyama, T. (2017). Learning in the Rodent Motor Cortex. Annu. Rev. Neurosci. *40*, 77–97.

Petrini, E.M., Ravasenga, T., Hausrat, T.J., Iurilli, G., Olcese, U., Racine, V., Sibarita, J.B., Jacob, T.C., Moss, S.J., Benfenati, F., et al. (2014). Synaptic recruitment of gephyrin regulates surface GABAA receptor dynamics for the expression of inhibitory LTP. Nat. Commun. *5*, 3921.

Pirker, S., Schwarzer, C., Czech, T., Baumgartner, C., Pockberger, H., Maier, H., Hauer, B., Sieghart, W., Furtinger, S., and Sperk, G. (2003). Increased expression of GABA(A) receptor beta-subunits in the hippocampus of patients with temporal lobe epilepsy. J. Neuropathol. Exp. Neurol. *62*, 820–834.

Pöltl, A., Hauer, B., Fuchs, K., Tretter, V., and Sieghart, W. (2003). Subunit composition and quantitative importance of GABA(A) receptor subtypes in the cerebellum of mouse and rat. J. Neurochem. *87*, 1444–1455.

Reijmers, L.G., Perkins, B.L., Matsuo, N., and Mayford, M. (2007). Localization of a stable neural correlate of associative memory. Science *317*, 1230–1233.

Ressler, R.L., and Maren, S. (2019). Synaptic encoding of fear memories in the amygdala. Curr. Opin. Neurobiol. *54*, 54–59.

Russ, J.C. (2006). The Image Processing Handbook, Fifth Edition (CRC Press).

Sangha, S., Ilenseer, J., Sosulina, L., Lesting, J., and Pape, H.C. (2012). Differential regulation of glutamic acid decarboxylase gene expression after extinction of a recent memory vs. intermediate memory. Learn. Mem. *19*, 194–200.

Schönherr, S., Seewald, A., Kasugai, Y., Bosch, D., Ehrlich, I., and Ferraguti, F. (2016). Combined optogenetic and freeze-fracture replica immunolabeling to examine input-specific arrangement of glutamate receptors in the mouse amygdala. J. Vis. Exp. *110*, e53853.

Smith, K.S., Engin, E., Meloni, E.G., and Rudolph, U. (2012). Benzodiazepine-induced anxiolysis and reduction of conditioned fear are mediated by distinct GABAA receptor subtypes in mice. Neuropharmacology *63*, 250–258.

Soltesz, I., Smetters, D.K., and Mody, I. (1995). Tonic inhibition originates from synapses close to the soma. Neuron *14*, 1273–1283.

Tovote, P., Fadok, J.P., and Lüthi, A. (2015). Neuronal circuits for fear and anxiety. Nat. Rev. Neurosci. *16*, 317–331.

Trouche, S., Sasaki, J.M., Tu, T., and Reijmers, L.G. (2013). Fear extinction causes target-specific remodeling of perisomatic inhibitory synapses. Neuron *80*, 1054–1065.

Turrigiano, G. (2012). Homeostatic synaptic plasticity: local and global mechanisms for stabilizing neuronal function. Cold Spring Harb. Perspect. Biol. *4*, a005736.

Villa, K.L., Berry, K.P., Subramanian, J., Cha, J.W., Oh, W.C., Kwon, H.-B., Kubota, Y., So, P.T.C., and Nedivi, E. (2016). Inhibitory synapses are repeatedly assembled and removed at persistent sites in vivo. Neuron *89*, 756–769.

Wang, W., Nakadate, K., Masugi-Tokita, M., Shutoh, F., Aziz, W., Tarusawa, E., Lorincz, A., Molnár, E., Kesaf, S., Li, Y.Q., et al. (2014). Distinct cerebellar

engrams in short-term and long-term motor learning. Proc. Natl. Acad. Sci. USA *111*, E188–E193.

Whittle, N., Hauschild, M., Lubec, G., Holmes, A., and Singewald, N. (2010). Rescue of impaired fear extinction and normalization of cortico-amygdala circuit dysfunction in a genetic mouse model by dietary zinc restriction. J. Neurosci. *30*, 13586–13596.

Wolff, S.B., Gründemann, J., Tovote, P., Krabbe, S., Jacobson, G.A., Müller, C., Herry, C., Ehrlich, I., Friedrich, R.W., Letzkus, J.J., and Lüthi, A. (2014). Amygdala interneuron subtypes control fear learning through disinhibition. Nature *509*, 453–458.

Yang, Y., Liu, D.Q., Huang, W., Deng, J., Sun, Y., Zuo, Y., and Poo, M.M. (2016). Selective synaptic remodeling of amygdalocortical connections associated with fear memory. Nat. Neurosci. *19*, 1348–1355.

Yuste, R., and Bonhoeffer, T. (2001). Morphological changes in dendritic spines associated with long-term synaptic plasticity. Annu. Rev. Neurosci. *24*, 1071–1089.

STAR★METHODS

KEY RESOURCES TABLE

REAGENT or RESOURCE	SOURCE	IDENTIFIER
Antibodies		
VGAT	Millipore	Cat# AB5062P (Lot# JC1604260); RRID: AB_2301998
$GABA_A$ R γ2 N-terminal	Synaptic Systems	Cat# 224 003 Lot# 224003/3); RRID: AB_2263066
Polyclonal rabbit anti-$GABA_A$ R γ2 intracellular loop, aa 319-366 of the rat sequence.	Pirker et al. (2003)	N/A
Polyclonal rabbit anti-$GABA_A$ R α2 intracellular loop, aa 322-357 of the rat sequence.	Pöltl et al. (2003) Kasugai et al. (2010)	N/A
Polyclonal rat anti-$GABA_A$ R α1 intracellular loop, aa 328-382 of the rat sequence.	Kasugai et al. (2010)	N/A
Chemicals		
[^{3}H]- Flunitrazepam	PerkinElmer	Cat# NET567
Software and Algorithms		
Mini Analysis Program	Synaptosoft	http://www.synaptosoft.com/MiniAnalysis/
Graphpad Prism	Graphpad	https://www.graphpad.com
SPSS	IBM	https://www.ibm.com/products/spss-statistics
Deposited Data		
Data deposited at Mendeley Data	This paper	https://doi.org/10.17632/gnn4rvxbr8.2
Other		
High-pressure freezing machine	Bal-Tec	Cat# HPM 010
Freeze-etching device	Bal-Tec	Cat# BAF 060
Experimental Models: Organisms/Strains		
Mouse: C57BL/6	Charles River	Strain Code 027

LEAD CONTACT AND MATERIALS AVAILABILITY

Further information and requests for reagents may be directed to, and will be fulfilled by the corresponding author, Dr. Francesco Ferraguti (Francesco.ferraguti@i-med.ac.at). For specific requests concerning non-commercial antibodies against $GABA_A$ receptor subunits requests may be directed to Dr. Werner Sieghart (Werner.Sieghart@meduniwien.ac.at).

EXPERIMENTAL MODEL AND SUBJECT DETAILS

Male C57BL/6 mice (Charles River, Sulzfeld, Germany or Füllinsdorf, Switzerland) were used for all experiments. All animal procedures were executed in compliance with institutional guidelines and were approved by the Austrian Animal Experimentation Ethics Board or Veterinary Department of the Canton of Basel-Stadt.

Twelve weeks-old mice group-housed in single ventilated cages were used for FRIL, *in situ* hybridization and autoradiography, whereas for electrophysiology experiments, seven to nine weeks-old single housed animals were used. All animals were kept in a temperature controlled room with a 12/12 h light/dark cycle.

METHOD DETAILS

Fear conditioning

Fear conditioning and extinction for FRIL, *in situ* hybridization and autoradiography were performed as previously described (Whittle et al., 2010). Twelve week-old male mice were fear conditioned in a 26 × 30 × 32 cm chamber with transparent walls and a metal rod floor (context A). After a 120 s acclimation period, an 80 dB white noise [conditioned stimulus (CS)] lasting 30 s was paired in the last 2 s with a 0.7 mA scrambled footshock [unconditioned stimulus (US)] five times (120 s interpairing interval). Control mice were

exposed to the CS-only. Mice were returned to the home cage after a 120 s no-stimulus consolidation period. Fear retrieval and extinction training sessions (20 CS presentations, 5 s no-stimulus interval) were performed 24 h after the conditioning in a novel context with different visual and olfactory cues. One group of control mice was exposed to 20 additional CS after 24 h from the first 5 CS presentation. Freezing behavior, defined as the absence of movement except respiration for at least 2 s, was manually scored from video recordings.

For electrophysiology experiments, mice were subjected to an auditory fear-conditioning paradigm with 5 CSs (7.5 kHz, 30 × 50 ms pips, 80 dB), each preceding one US (mild footshock, 0.6 mA, 1 s) as previously described (Herry et al., 2008). In order to deliver tone/shock pairings, a current generator and scrambler was controlled by a computer running the TruScan 99 software (Coulbourn Instruments, Allentown, PA). Fear retrieval and extinction were performed in a new context with different visual and olfactory cues. Fear retrieval was performed 24 hours after conditioning, whereas extinction included two training sessions of 20 CSs performed at 24 and 48 hours after the conditioning. Freezing behavior was quantified during each behavioral session by an automatic infrared beam detection system (Coulbourn Instruments)(Herry et al., 2008).

Pre-embedding electron microscopy

Twelve week-old male mice (n = 2) were deeply anesthetized by intraperitoneal injection of thiopental (150 mg/kg, i.p) and perfused transcardially with phosphate buffered saline (PBS; 25 mM, 0.9% NaCl, pH 7.4) followed by ice-cold fixative made of 4% w/v paraformaldehyde and 15% v/v of a saturated solution of picric acid in phosphate buffer (PB; 0.1 M, pH 7.4) for 10 min. Glutaraldehyde was added to the fixative at a final concentration of 0.05% v/v just before perfusion. Brains were immediately removed from the skull, washed in 0.1 M PB and sliced coronally in 70 μm thick sections on a vibratome (Leica Microsystems VT1000S, Vienna, Austria). Free floating sections were cryoprotected in 20% w/v sucrose made in 0.1M PB overnight at 4°C and then freeze-thawed twice to allow antibody penetration. Pre-embedding immunoperoxidase reactions were carried out as described previously (Dobi et al., 2013) using the avidin-biotin-HRP complex method (ABC, Elite kit, Vector Laboratories, Burlingame, CA). Identification of GABAergic terminals was obtained using an anti-vesicular GABA transporter (VGAT) antibody (Millipore, Cat. No. AB5062P, Lot. No. JC1604260) diluted 1:2,500. Portions of the BA were dissected under a stereomicroscope and re-embedded. Serial ultrathin sections (70 nm) were cut with a diamond knife on an ultramicrotome (Ultracut S; Leica, Vienna, Austria) and collected on formvar-coated copper slot grids. The ultrastructural analysis of the specimens was performed using a Philips CM 120 electron microscope equipped with a Morada CCD-TEM camera (Soft Imaging Systems). 3D reconstruction of GABAegic synapses was performed using the Neurolucida software (MBF Bioscience) and the synaptic area measurements with Neurolucida Explorer.

Freeze-fracture replica immunolabeling

Only 5 animals/group/experiment were processed for FRIL, and were selected among those with the best behavioral response. FRIL was performed according to previously published procedures (Kasugai et al., 2010; Schönherr et al., 2016). Mice were transcardially perfused with PB (0.1 M, pH 7.4) followed by a fixative containing 1% formaldehyde and 15% of a saturated solution of picric acid for 12 min. Forebrains were cut into 140 μm thick coronal sections with a Vibroslicer (Leica Microsystems VT1000S) from where BA samples were dissected out under a stereomicroscope, cryoprotected overnight with 30% glycerol and then frozen with a high-pressure freezing machine (HPM 010; Bal-Tec, Balzers, Liechtenstein). Frozen specimens were fractured and replicated by evaporation of carbon and platinum using a freeze-etching device (BAF 060; Bal-Tec). Tissue was solubilized in a solution containing 2.5% sodium lauryl sulfate (SDS) and 20% sucrose made up in 15 mM Tris buffer, pH 8.3, with shaking for 18 h at 80°C. Replicas were kept in the same solution at RT until processed further. Before immunolabeling, replicas were preincubated in a blocking solution containing 5% BSA in TBS for 1 h at RT, and then incubated in primary antibodies diluted in TBS containing 2% BSA and 2% normal goat serum (NGS), overnight at 6°C. After a final wash in MilliQ water, replicas were mounted on formvar-coated 100-line copper grids. Somatic and dendritic GABAergic synapses were randomly sampled and analyzed by an experimenter blind to the experimental group. Digital electron micrographs of synapses were taken at a magnification of 53k with a Philips CM120 transmission electron microscope (TEM) equipped with a Morada CCD camera (Soft Imaging Systems, Münster, Germany).

Image analysis of electron microscopy images

Synapses were collected from 2 replica/mouse. For the quantification of the GABA-PSA, only synapses for which the entire IMP cluster could be identified were analyzed. For receptor density measures also partial synapses (in which the IMP cluster on the P-face of the plasma membrane was in part covered by the E-face of the plasma membrane of the presynaptic axon) were evaluated. Inclusion criteria for full synapses were: a cluster composed of > 10 IMPs, an area > 0.010 μm^2 and labeled by at least 3 gold particles. In one animal/group, synapses were oversampled to control for reliability of the sampling. Random sampling was then applied for further statistical comparisons to achieve a similar sample size among subjects and groups. The extrasynaptic area analyzed was the area of the plasma membrane adjacent to the IMP clusters and present within the 53k digital images of the synapses. Analysis of the synaptic area and density of gold particles was performed offline using the ImageJ 1.45 s software (NIH, USA) by investigators blind to the treatment groups. Analysis of the shape of synapses was performed with the same imaging software using shape descriptors: form factor, roundness and solidity (Russ, 2006).

In order to analyze the intrasynaptic distribution of gold particles, we developed a novel analysis procedure based on the identification of the center of gravity of synapses, alignment based on minor and major axis passing through the center of gravity, and

scaling to the average synaptic area and shape determined for each experimental group (Figure S3). The respective locations of gold particles in the synaptic area were then marked in the standard synapse to generate a heatmap (Figure 3E; Figure S3C) with ImageJ 1.45 s (NIH, USA) including ImageJ plug-in software, Image stack merger plus developed by Dr. Samuel Péan (http://www.samuelpean.com/image-stack-merger-plus/).

Brain slice electrophysiology

Three h after behavioral training, animals were anesthetized with isoflurane and decapitated as previously described (Bissière et al., 2003). Briefly, brains were dissected in ice-cold artificial cerebrospinal fluid (ACSF), and coronal slices (300 μm thick) were sectioned at 4°C with a vibratome (Microm HM 650 V; Walldorf, Germany). Slices were allowed to recover for 45 min at 37°C in an interface chamber containing ACSF equilibrated with 95% O_2/5% CO_2. The ACSF contained (in mM): 124 NaCl, 2.7 KCl, 2 $CaCl_2$, 1.3 $MgCl_2$, 26 $NaHCO_3$, 0.4 NaH_2PO_4, 18 glucose, 2.25 ascorbate. Neurons were visually identified with infrared video microscopy using an upright microscope equipped with x5 and x40 objectives (Olympus, Germany). Whole-cell patch-clamp recordings were obtained from projection neurons in the BA at 32°C in a submerged chamber under constant superfusion with ACSF. Patch electrodes (4.5 - 5.5 MΩ) were pulled from borosilicate glass tubing and filled with an intracellular solution consisting of (in mM): 130 KCl, 10 HEPES, 10 phosphocreatine Na_2, 4 Mg-ATP, 0.4 Na-GTP (pH adjusted to 7.25 with KOH, ~290 – 300 mOsm). The membrane potential was held at −80 mV in voltage-clamp recordings. In order to block glutamatergic synaptic transmission all recordings were performed in the presence of CPP (20 μM), CNQX (20 μM) and TTX (1 μM). Data were acquired with pClamp9 (Molecular Devices) and recorded with a Multiclamp 700A amplifier (Molecular Devices). Data were sampled at 20 kHz and filtered at 2 kHz. Series resistance was monitored every 3 min by applying a –5 mV hyperpolarizing pulse. If during an experiment series resistance changed more than 20%, or exceeded 20 MΩ, recordings were discarded. No differences in series resistance was detected among groups (Figure S6A). mIPSC recordings were achieved in the gap-free modus. For each neuron, at least 276 mIPSC events were recorded. Frequency, amplitude, charge transfer and kinetics of mIPSC were analyzed offline using the Mini Analysis Program (version 6.0.9, Synaptosoft). The threshold for mIPSC detection was set to 27 pA.

In situ hybridization

Mice used for *in situ* hybridization and autoradiography were killed by decapitation 2 hours after fear conditioning or extinction. Their brains were quickly removed from the skull, frozen in isopentane at −30 to −40°C for 1 min, and then stored at −80°C. Sections of the amygdala were cut at a thickness of 15 μm using a HM 560 Microm cryostat and mounted onto poly-L-lysine-coated Superfrost glass slides (Roth, Karlsruhe, Germany). Every 7th section was Nissl stained and a series of matching sections were selected for subsequent *in situ* hybridization or autoradiography experiments.

In situ hybridization was performed as described previously in detail (Hörtnagl et al., 2013). Oligonucleotides for $GABA_A$ receptor α_1 subunit: 5′ CCT GGC TAA GTT AGG GGT ATA GCT GGT TGC TGT AGG AGC ATA TGT 3′, $GABA_A$ receptor α_2 subunit: 5′ CAT CGG GAG CAA CCT GAA CGG AGT CAG AAG CAT TGT AAG TCC 3′ and $GABA_A$ receptor γ_2 subunit: 5′ GGC AAT GCG AAT ATG TAT CCT CCC ATG TCT CCA GGC TCC TGT TCG GC 3′ (Microsynth, Balgach, Switzerland, 2.5 pmol) were 3′ end-labeled by [^{35}S]α-dATP (50 μCi; 1300 Ci/ mmol, Hartmann Analytic GmbH, Braunschweig, Germany) and terminal transferase (Roche Diagnostics, Basel, Switzerland). Hybridization was performed in 50% formamide, 4x SSC (1x SSC is 150 mM NaCl, 15 mM sodium citrate, pH 7.2), 500 μg/ml salmon sperm DNA, 250 μg/ml yeast tRNA, 1x Denhardt's solution (0.02% Ficoll, 0.02% polyvinylpyrrolidone, and 0.02% bovine serum albumin), 10% dextran sulfate, and 20 mM dithiothreitol (all from Sigma) at 42°C for 18 hours. Sections were washed at stringent conditions (50% formamide in 2x SSC, 42°C). Slides were exposed to BioMax MR films (Amersham Pharmacia Biotech, Buckinghamshire, UK) together with [^{14}C]-microscales for 7 to 14 days. Quantitative evaluation of relative optical density of *in situ* hybridization was done using 8 bit digitized images of the autoradiographs and the ImageJ 1.45 s software. Data are presented as percentage of controls by an experimenter blind to the experimental group.

Autoradiography

For localization of benzodiazepine-sensitive $GABA_A$ receptors in the amygdala, [^{3}H]-Flunitrazepam (84.9 Ci/mmol; PerkinElmer, Boston, USA) was used. The slice autoradiography experiments were performed as previously described (Heldt and Ressler, 2007) with minor modifications. Brain sections (15 μm thick) were thawed and dried at room temperature and preincubated for 2x10 min at 4°C in buffer containing 50 mM Tris and 1 mM EDTA (pH 7.4) to wash out the intrinsic GABA. Tissue sections were then transferred in the incubation buffer (50 mM Tris, 120 mM NaCl; pH 7.4) for 15 min at 4°C. The sections were incubated for 60 min at 4°C in incubation buffer containing 15 nM [^{3}H]-Flunitrazepam. The sections were subsequently rinsed 2x30 s in ice-cold incubation buffer and then dipped in ice-cold distilled water. They were immediately dried using a hair-drier. Dried sections were exposed to Biomax MR Kodak autoradiography film (Sigma Aldrich) for 6 days at room temperature in the dark. To each film tritium-micro-scale standards (GE Healthcare Amersham, UK) were added. The films were developed using Kodak developer (Sigma Aldrich) and subsequently fixed using Kodak solution (Sigma Aldrich). The films were scanned with a computer scanner at 600 dpi and analyzed. To determine the unspecific binding, flumazenil in 1,000-fold concentration of the [^{3}H]-Flunitrazepam was added to the incubation jar. Quantitative evaluation of the relative optical density was done using the digitized images of the autoradiographs with ImageJ 1.45 s by an experimenter blind to the experimental group.

QUANTIFICATION AND STATISTICAL ANALYSIS

Data were analyzed with the Prism 7 (GraphPad Software Inc.) or SPSS software. Sample size was predetermined on the basis of published studies, experimental pilots and in-house expertise. Animals were randomly assigned to experimental groups. Data are shown as boxplots (median, mean and quartiles) with whiskers indicating minimum and maximum values. Single data points are also plotted alongside the boxplots. Data distribution was tested for normality, and consequently analyzed with appropriate parametric or non-parametric statistical tests (e.g., two-tailed Mann-Whitney or Kruskal-Wallis tests). Where applicable, significant effects were further analyzed using post hoc tests. Cumulative frequency distributions were analyzed by means of the two-sample Kolmogorov–Smirnov test. To obtain the delta percentage between frequency distributions, we first averaged the medians of the synaptic area for the two groups. This average value was then used as the cut-off. P values less than 0.05 were considered statistically significant. Statistical details related to both main and supplementary figures can be found in Table S1 "Statistical tables related to figures."

DATA AND CODE AVAILABILITY

The datasets generated during this study are available at Mendeley Data: https://doi.org/10.17632/gnn4rvxbr8.2.